ACHIEVING HIGH SPIN-FLIP EFFICIENCY WITH AN RF MAGNET AND DISCOVERY OF SPIN-RESONANCE STRENGTH FORMULAE PROBLEM

by

Maria A. Leonova

A dissertation submitted in partial fulfillment
of the requirements for the degree of
Doctor of Philosophy
(Physics)
in The University of Michigan
2008

Doctoral Committee:

Professor Alan D. Krisch, Chair
Professor Georg A. Raithel
Emeritus Professor Byron P. Roe
Professor York-Peng E. Yao
Associate Professor Eitan Geva

For my family

ACKNOWLEDGEMENTS

I would like to thank the entire COSY, IUCF and MIT-Bates staffs for the successful operation of COSY COoler SYnchrotron, the IUCF Cooler Ring and the MIT-Bates Storage Ring, and their injectors and polarized sources. I also thank my collaborators on the experiments discussed in this thesis. I am grateful to the late Professor Yuri Ado of IHEP-Protvino for introducing me to Accelerator Physics. I want to thank my advisor, Professor Alan Krisch, for his help and advice through my graduate studies. Finally, I thank my husband Vasily and my mother for their encouragement and support.

TABLE OF CONTENTS

LIST OF TABLES

LIST OF FIGURES

Figure

ABSTRACT

ACHIEVING HIGH SPIN-FLIP EFFICIENCY WITH AN RF MAGNET AND DISCOVERY OF SPIN-RESONANCE STRENGTH FORMULAE PROBLEM

by

Maria A. Leonova

Chairman: Alan D. Krisch

Frequent polarization reversals, or spin-flips, of a beam in high energy storage rings, may be a powerful tool for greatly reducing the systematic errors of spin asymmetry measurements in scattering experiments. A spin-flipping technique using an artificially induced spin-depolarizing resonance, created by an rf magnet with a horizontal magnetic field, is being developed to allow such polarization reversals in a well-controlled way. We used a new ferrite rf dipole to study the spin flipping of a 2.1 GeV/c vertically polarized proton beam stored in the COSY Cooler Synchrotron in Jülich, Germany. We swept the rf dipole's frequency through an rf-induced spin resonance to flip the beam's polarization direction. After determining the resonance's frequency, we varied the frequency's range and ramp time, and the number of flips. At the rf dipole's maximum strength and its optimum frequency range and ramp time, we measured a proton spin-flip efficiency of $99.92 \pm 0.04\%$. This result, along

with previous similar IUCF results at lower energy, indicate that due to the Lorentz invariance of an rf-dipole's transverse $\int Bdl$ and the weak energy dependence of its spin-resonance strength, a small rf dipole should allow efficient spin flipping in very high energies in rings such as the 250 GeV RHIC or even the 7 TeV LHC.

The accurate prediction of a spin-depolarizing resonance strength remains a challenge. We earlier analyzed all available data on the spin-flipping of stored beams of polarized protons, electrons and deuterons. We found 10-20-fold deviations of the measured rf-induced resonance strength from the theoretically predicted strength. Therefore, we recently studied these resonance strength deviations experimentally by varying the rf dipole's voltage, and the size, momentum spread and vertical betatron tune with a 2.1 GeV/c polarized proton beam stored in COSY. We found no dependence of the resonance strength on the beam's size or momentum spread. We did find enhancements of more than 100 when the rf spin resonance was near an intrinsic proton spin resonance.

We also studied the resonance strength deviations experimentally by using 1.85 GeV/c vertically polarized deuterons stored in COSY with an rf dipole and then an rf solenoid. We found no dependence on the beam's size or momentum spread, or on the rf frequency sweep range for either the rf dipole or rf solenoid. We saw a significant enhancement of the rf spin resonance strength ε near an intrinsic spin resonance with the rf dipole, but no enhancement with the rf solenoid, except exactly at the position of the very narrow intrinsic resonance. For an rf dipole the deuteron resonance strength appeared to be about seven times smaller than expected. This resonance strength reduction does not seem to affect the maximum spin-flip efficiency, but it does require a very large frequency ramp time to achieve high spin-flip efficiency. Moreover, these results indicated that for rf dipoles the widely used resonance strength formula appeared to be incorrect. Thus, further studies of rf-magnet-induced spin resonance strengths are underway at COSY for both proton and deuteron beams.

CHAPTER I

INTRODUCTION

Spin is considered a fundamental property of nuclei and subnuclear particles; it appears naturally in the Dirac equation. Experimental studies of the spin dependence of the strong interaction between elementary particles are needed to reveal new and important aspects of the strong interaction, which cannot be investigated with unpolarized beams and targets. Thus, these studies need polarized targets, polarized beams or both. During the past decade, polarized proton, electron, and deuteron beam experiments have become a major component of the programs in storage rings such as the IUCF Cooler Ring [1], AmPS at NIKHEF [2], the MIT-Bates Storage Ring [3], the COSY Cooler Synchrotron [4], LEP at CERN [5], RHIC at BNL [6] and HERA at DESY [7].

In an ideal flat storage ring or circular accelerator, each particle's spin precesses around the vertical magnetic fields of the ring's bending dipoles. The number of these precessions during one turn around the ring, called the spin tune, is proportional to particle's energy and is given by

$$\nu_s = G\gamma, \tag{I.1}$$

where γ is particle's Lorentz factor and G is its gyromagnetic anomaly (for protons $G_p = 1.792847$ and for deuterons $G_d = -0.142987$).

With no horizontal magnetic field the vertical spin motion is stable, and a beam's polarization remains unchanged; but the spin motion will be perturbed by any horizontal magnetic field. A spin-depolarizing resonance occurs whenever a periodic horizontal magnetic field's frequency becomes synchronized with the spin precession frequency; this allows the perturbations to add up constructively over a large number of turns and cause depolarization. The condition for a depolarizing resonance in terms of the betatron tunes is

$$\nu_s = l\nu_x + m\nu_y + n, \tag{I.2}$$

where ν_x and ν_y are the horizontal and vertical betatron tunes, respectively, while l, m and n are integers. When $l = m = 0$, the resonance is called an "imperfection resonance", which occurs because of the imperfections in the ring's magnetic structure. When either l or m or both are different from 0, the resonance is called an "intrinsic resonance", which is caused by the horizontal magnetic fields of the ring's focusing quadrupoles. Since the spin tune is proportional to the particle's energy, the higher the beam energy, the more resonances must be overcome to preserve beam's polarization during acceleration. Many techniques [8, 9, 10, 11, 12, 13, 14, 15, 16] have been developed to overcome depolarizing resonances.

The measurements of asymmetries in polarized scattering experiments have systematic errors that can be significantly reduced by frequent reversals of the beam's polarization direction. Spin reversals can be achieved using either an rf solenoid's longitudinal magnetic field or an rf dipole's transverse magnetic field. Running an rf magnet at a frequency near the spin precession frequency, can create one or more rf-induced spin-depolarizing resonances; the spin direction can then be flipped by ramping the rf magnet's frequency through one of these resonance's central frequency. The frequency f_r of such an artificially rf-induced spin-depolarizing resonance is:

$$f_r = f_c(k \pm \nu_s), \tag{I.3}$$

where f_c is the particle's circulation frequency, k is an integer and ν_s is the spin tune.

Varying the rf magnet's frequency from a value below f_r, to a value above it, is called crossing the resonance. After such a crossing, the final beam polarization P_f is related to the initial beam polarization P_i by the Froissart-Stora equation [17]

$$P_f = P_i \left\{ 2\ exp\left[\frac{-(\pi \mathcal{E} f_c)^2}{\Delta f/\Delta t} \right] - 1 \right\}, \tag{I.4}$$

where $\mathcal{E}$ is the resonance strength, and $\Delta f/\Delta t$ is the resonance crossing rate, while Δf is the frequency's ramp range during its ramp time Δt. The value of the exponent determines the final polarization. If the resonance is very strong and/or the crossing rate is very slow, then the exponent is very large and the exponential approaches zero; therefore, the final polarization is reversed with respect to the initial polarization, while its absolute value is the same. This is called a spin flip.

Such a 180° spin rotation by an rf dipole's magnetic field was shown to be practical at high energies [18, 19, 20, 21, 22, 23, 24], because it is energy independent. However, the spin rotation due to a solenoid's magnetic field decreases linearly with the beam's energy because of the Lorentz contraction of its $\int Bdl$; thus, an rf solenoid would have to be impractically long for spin-flipping in very high energy rings. Therefore, we built and installed a water-cooled ferrite-core rf dipole in the COSY Cooler Synchrotron

ring at the Forschungszentrum in Jülich, Germany, with a high rf-magnetic field and, thus, a high induced resonance strength ε. We used it to study the spin-flipping of 2.1 GeV/c vertically polarized protons stored in the COSY ring. We swept the rf dipole's frequency through an rf-induced spin resonance; after optimizing the sweep parameters, we used multiple spin flipping to measure a spin-flip efficiency of $99.92 \pm 0.04\%$.

The Michigan Spin Physics Center has carried out many experimental studies of accelerating, storing and manipulating spin-polarized proton and deuteron beams at the IUCF Cooler Ring [18, 19, 20, 21, 22, 25, 26, 27, 28] and at COSY [23, 24, 29, 30], and of electron beams at the MIT-Bates Storage Ring [31]. Spin-flipping data obtained by the Spin Physics Center and collaborators at these rings show that the experimentally measured rf-induced resonance strength often does not agree with the strength calculated from each rf magnet's $\int B \cdot dl$ and the equations used for many years. Understanding this disagreement is important for the correct estimation of the rf magnet's strength required for efficient spin flipping; it is also important for properly understanding spin motion in storage rings and accelerators.

The first part of this thesis describes a high efficiency spin-flipping experiment using a stored polarized proton beam at COSY [32]. The second part investigates the strength of an rf-induced spin-depolarizing resonance [33, 34]. Since this subject remains a challenge theoretically, my goal in this experimental thesis is to present the data and to indicate some possible directions for the still-developing theory.

Chapter II contains a very brief discussion of polarized beam theory, with emphasis on rf-induced depolarizing resonances and spin-flipping. Chapter III describes the experimental apparatus, including the COSY Cooler Synchrotron, and the COSY-Michigan rf dipole and rf solenoid. Chapter IV describes the high efficiency proton spin-flipping experiment. Chapter V contains an overview of all spin-flipping data that we know of, and discusses studies of the rf-dipole induced spin-depolarizing resonance strength done with protons and deuterons at COSY, and studies of the rf-solenoid induced spin resonance strength done with deuterons at COSY. Finally, Chapter VI contains the conclusions.

CHAPTER II

THEORETICAL MOTIVATION

II.1 Spin Motion and Spin Resonances

The spin of a particle interacts with an electromagnetic field through the magnetic moment associated with the spin. Let $\vec{S}$ be the spin represented as a 3-vector; the associated magnetic moment is

$$\vec{\mu} = \frac{ge}{2m}\vec{S}, \tag{II.1}$$

where g is the gyromagnetic ratio, e is particle's charge, and m is its mass in its rest frame. For an ideal Dirac particle, g is exactly equal to 2. The deviation of g from 2, which is called the "anomalous" magnetic moment of the particle, can be specified by a parameter G called the gyromagnetic anomaly

$$G = \frac{g-2}{2}. \tag{II.2}$$

For electrons and muons, the value of G is approximately equal to the fine structure constant $\alpha = 1/137$ divided by 2π. More precisely it is given by

$$G = \begin{cases} 0.001159657, & \text{electron} \\ 0.001165924, & \text{muon} \end{cases}; \tag{II.3}$$

while for a proton $G_p = 1.792847$, and for a deuteron $G_d = -0.142987$.

II.1.1 Thomas-BMT Equation

Consider a particle of mass m and charge e at rest in a magnetic field $\vec{B}$. The spin motion is a precession of the spin vector $\vec{S}$ around the magnetic field direction $\vec{B}$, with the equation of motion [35, 36]

$$\frac{d\vec{S}}{dt} = \vec{\Omega} \times \vec{S}; \tag{II.4}$$

the spin precession's angular velocity $\vec{\Omega}$ is

$$\vec{\Omega} = -\frac{ge}{2m}\vec{B}. \tag{II.5}$$

Eqs. (II.4) and (II.5) describe the spin precession of a stationary particle, but we need an equation for a relativistic particle moving in the electromagnetic fields $\vec{E}$ and $\vec{B}$ of an accelerator ring. Let $\vec{v}$ be the instantaneous velocity of the particle; then, to consider the precession of a moving particle as the precession of a stationary particle in a moving frame, one must make a Lorentz transformation to the particle's rest frame. In this frame the spin precession equation is still Eq. (II.4); however $\vec{\Omega}$ needs to be transformed. Note that $\vec{S}$ is only well defined in the particle's rest frame, while all other quantities, $\vec{E}$, $\vec{B}$, $\vec{v}$ and time t, can be defined in the laboratory frame and then transformed into the particle's rest frame.

The orbital motion of a charged particle moving in the electromagnetic fields $\vec{E}$ and $\vec{B}$ can be expressed as [35]

$$\frac{d\vec{v}}{dt} = -\frac{e}{m\gamma}\left[\vec{B} + \frac{\gamma^2}{\gamma^2+1}\frac{\vec{E}\times\vec{v}}{c^2}\right]\times\vec{v}, \tag{II.6}$$

where γ is the relativistic energy factor and c is the speed of light.

Transforming the magnetic field into particle's rest frame, inserting it into Eq. (II.5), and then transforming back to the laboratory frame, one obtains

$$\vec{\Omega} = -\frac{e}{m\gamma}\left[(G\gamma+1)\,\vec{B}_\perp + (1+G)\vec{B}_\parallel - \left(G\gamma + \frac{\gamma}{\gamma+1}\right)\frac{1}{c}\vec{\beta}\times\vec{E}\right], \tag{II.7}$$

which, when substituted into Eq. (II.4), is called the Thomas-BMT equation [37, 38], where BMT stands for Bargman, Michel, and Telegdi. The effect of the electric field $\vec{E}$ on spin motion is usually negligible in circular accelerators; thus, the last terms in both, Eq. (II.6) and (II.7) can be ignored.

In Eq. (II.7), the "1" in $(G\gamma+1)\,\vec{B}_\perp$ is due to the Thomas precession, which appears because the particle is accelerated radially. The origin of the Thomas precession is non inertial relativistic kinematics. One can see that two successive Lorentz transformations along $\vec{\beta}_1$ and $\vec{\beta}_2$ can be combined into a single Lorentz transformation only if $\vec{\beta}_1$ is parallel to $\vec{\beta}_2$. Otherwise, they can only be combined into a Lorentz transformation plus a rotation; this additional rotation is the Thomas precession.

II.1.2 Spin Dynamics Using Quantum Mechanical Spinor Formalism

In a circular accelerator, it is sometimes convenient to replace the time variable t with the particle's orbital angle θ. The transformation between θ and t is defined by

$$d\theta = \frac{v}{\rho}dt, \tag{II.8}$$

where ρ is the local radius of curvature of the particle's orbit and υ is its velocity.

One can analyze the spin dynamics in the periodic magnetic structure of a synchrotron using the spinor algebra language [36, 39, 40, 41]. where the spin is represented by a complex 2-component vector ψ, with

$$\vec{S} = \psi^{\dagger}\vec{\sigma}\psi, \tag{II.9}$$

where $\vec{\sigma}$ denotes the Pauli matrices with components

$$\sigma_x = \begin{pmatrix} 0 & 1 \\ 1 & 0 \end{pmatrix}, \quad \sigma_l = \begin{pmatrix} 0 & -i \\ i & 0 \end{pmatrix}, \quad \sigma_y = \begin{pmatrix} 1 & 0 \\ 0 & -1 \end{pmatrix}, \tag{II.10}$$

where $\hat{x}$, $\hat{l}$ and $\hat{y}$ are the radial, longitudinal and vertical axes, respectively.

In terms of the orbital angle θ and two-component spinor ψ, the Thomas-BMT equation [37, 38] of spin motion then describes the time evolution of ψ [36, 41]

$$\frac{d\psi}{d\theta} = -\frac{i}{2}\begin{pmatrix} G\gamma & -\zeta \\ -\zeta^* & -G\gamma \end{pmatrix}\psi, \tag{II.11}$$

where the diagonal matrix elements $G\gamma$ describe spin precession around the vertical fields of the bending dipoles while the off-diagonal element ζ characterizes the spin-perturbing kick, which couples the spinor's up ($\psi_{\uparrow}$) and down ($\psi_{\downarrow}$) components. The quantity ζ is given by [36]

$$\zeta = (1 + G\gamma)\frac{\tilde{B}_x}{B} + (1 + G)\frac{\tilde{B}_l}{B}, \tag{II.12}$$

where $\tilde{B}_x$ and $\tilde{B}_l$ are the radial and longitudinal perturbing fields, respectively.

Because of the periodic nature of a particle's motion in synchrotrons, ζ can be expanded in a Fourier series

$$\zeta(\theta) = \sum_{\kappa} \varepsilon_{\kappa} e^{-i\kappa\theta}, \tag{II.13}$$

where the Fourier amplitude ε_{κ} is called the resonance strength and the harmonic κ is called the resonance tune, which is the frequency of the spin-perturbing kicks. When the spin precession frequency is equal to the resonance tune ($\nu_s = \kappa$), then the beam may be depolarized by the coherent spin perturbations caused by these kicks.

The motion in the x and y directions contains harmonics of $(k \pm \nu_x)$ and $(k \pm \nu_y)$, respectively, due to the betatron oscillations, and harmonics of k due to closed orbit distortions, where ν_x and ν_y are the horizontal and vertical betatron tunes, respectively, and k is an integer. These terms contribute to perturbations of the spin motion, with perturbation tunes of $k \pm \nu_x$, $k \pm \nu_y$ and k, respectively.

II.1.3 Depolarization Resonances

Perturbations to the spin motion will accumulate, i.e. a spin resonance will occur, whenever the perturbations to the spin motion are in phase with the unperturbed spin motion. Thus, one expects a resonance to occur when one of these perturbation tunes is equal to the unperturbed tune, i.e. when

$$G\gamma = \begin{cases} k \pm \nu_y, & \text{for vertical deviation from a closed orbit due to vertical} \\ & \text{betatron oscillations,} \\ k, & \text{for transverse deviations due to closed orbit distortions.} \end{cases} \tag{II.14}$$

When a beam is injected into an accelerator, one aligns its spin along the vertical direction $\hat{y}$. An ideal particle, whose spin motion is simple precession around $\hat{y}$, would keep its spin aligned along $\hat{y}$. The hope is that the spin direction of the non-ideal particles would not deviate far from $\hat{y}$, so that the net polarization of the whole beam does not decrease significantly. This is not a problem if the perturbations are small, and are not in phase with the natural spin motion. However, when a depolarizing resonance occurs, even small perturbations can cause large deviations of the spin direction from $\hat{y}$ and the beam polarization can be lost. Therefore, the resonances in Eq. (II.14) are called spin-depolarizing resonances; they are the resonances which do not affect the particles' *orbital* motion.

Any horizontal magnetic fields can perturb the spin motion, and thus depolarize the beam. This depolarization occurs whenever the spin tune ν_s satisfies the depolarizing resonance condition:

$$\nu_s = l\nu_x + m\nu_y + n, \tag{II.15}$$

where l, m and n are integers. The imperfection depolarizing resonances occur when $l = m = 0$, while the intrinsic depolarizing resonances occur when either $l \neq 0$ or $m \neq 0$, or both. The sum of l and m defines the order of the resonance. For example, a resonance with $l = 1$ and $m = 2$ is a third-order resonance. Generally, the higher order depolarizing resonances are weaker.

The *imperfection* resonances come from the y-orbit distortions due to the imperfections in the ring magnets. By making good orbit corrections (sometimes called harmonic spin matching) these resonances can be reduced in strength. The *intrinsic* resonances come from the vertical betatron amplitudes of the particles, which move the particles into the focusing fields of quadrupoles with a component along $\hat{x}$, and thus perturb rotations around $\hat{x}$. Since any beam has a non-zero emittance, these resonances can not be avoided by any error correction scheme [36].

II.2 Spin Resonance Strength

II.2.1 Introduction

Consider the Thomas-BMT equation [37, 38] in a spinor representation [36, 41]

$$\frac{d\psi}{d\theta} = -\frac{i}{2}\begin{pmatrix} G\gamma & -\zeta \\ -\zeta^* & -G\gamma \end{pmatrix}\psi, \tag{II.16}$$

where the quantity ζ describes the spin perturbation and is given by

$$\zeta = (1+G\gamma)\frac{\tilde{B}_x}{B} + (1+G)\frac{\tilde{B}_l}{B} = \sum_{\kappa} \mathcal{E}_\kappa e^{-i\kappa\theta}. \tag{II.17}$$

One can use Eq. (II.17) to find the spin resonance strength $\mathcal{E}_\kappa$, which is defined as the Fourier amplitude of the κ harmonic [36]

$$\mathcal{E}_\kappa \equiv \frac{1}{2\pi}\oint \zeta(\theta) e^{i\kappa\theta} d\theta = \frac{1}{2\pi}\oint \left\{(1+G\gamma)\frac{\tilde{B}_x}{B} + (1+G)\frac{\tilde{B}_l}{B}\right\} e^{i\kappa\theta} d\theta. \tag{II.18}$$

II.2.2 RF-Induced Spin Resonance Strength

Consider a short rf dipole with a time-dependent radial magnetic field $B_x(t)$ given by

$$B_x(t) = B_{rf}\cos(2\pi f_{rf} t + \chi), \tag{II.19}$$

where B_{rf} is its oscillating magnetic field's amplitude, f_{rf} its frequency, and χ is an arbitrary phase. Assume that the rf dipole is the only source of the spin-perturbing radial magnetic field $\tilde{B}_x$ in Eq. (II.18) [42, 43, 44, 45, 46]. Each circulating particle encounters the rf dipole's field once on every turn. The spin-perturbing field $\tilde{B}_x$ can be written as a function of the total distance s traveled by the particle in the following way

$$\tilde{B}_x(s) = B_{rf}\cos(2\pi\nu_{rf}\frac{s}{L} + \chi)\sum_{n=-\infty}^{+\infty}\begin{cases} 1, & -(l/2)+nL < s < (l/2)+nL \\ 0, & \text{otherwise} \end{cases}, \tag{II.20}$$

where L is the ring's circumference, n is the number of particle turns, and l is the rf dipole's length. The quantity ν_{rf} is the rf tune, which is the number of the rf dipole field oscillations during one turn around the ring:

$$\nu_{rf} = f_{rf}/f_c, \tag{II.21}$$

where f_c is the beam's circulation frequency.

In the limit of a very short rf dipole ($l/L \to 0$), its spin-perturbing magnetic field $\tilde{B_x}(s)$ in Eq. (II.20) can be expressed as

$$\begin{aligned}\tilde{B_x}(s) &= \int B_{rf} dl \cos(2\pi\nu_{rf}\frac{s}{L} + \chi) \times \\ &\quad \sum_{n=-\infty}^{+\infty} \lim_{l\to 0} \begin{cases} 1/l, & -(l/2) < (s - nL) < (l/2) \\ 0, & \text{otherwise} \end{cases} \\ &= \int B_{rf} dl \cos(2\pi\nu_{rf}\frac{s}{L} + \chi) \sum_{n=-\infty}^{+\infty} \delta(s - nL), \end{aligned} \tag{II.22}$$

where $\delta(s - nL)$ is the Dirac delta function.

Converting the variable in Eq. (II.22) from the distance s to the orbital angle θ transforms Eq. (II.22) into

$$\tilde{B_x}(\theta) = \int B_{rf} dl \cos(\nu_{rf}\theta + \chi) \sum_{n=-\infty}^{+\infty} \frac{\delta(\theta - 2\pi n)}{\rho}, \tag{II.23}$$

where we used the relations $s = \theta\rho$, $L = 2\pi\rho$, and $\delta(\theta\rho - 2\pi n\rho) = \delta(\theta - 2\pi n)/\rho$.

Inserting Eq. (II.23) into Eq. (II.18) and using the identity

$$\cos(\nu_{rf}\theta + \chi) \sum_{n=-\infty}^{+\infty} \delta(\theta - 2\pi n) = \frac{1}{2\pi} \sum_{n=-\infty}^{+\infty} \cos[(\nu_{rf} + n)\theta + \chi] \tag{II.24}$$

gives the rf-dipole induced spin resonance strength

$$\mathcal{E}_{Bdl}^{dip} = \frac{(1+G\gamma)}{2\pi} \frac{\int B_{rf} dl}{B\rho} \oint \frac{1}{2\pi} \sum_{n=-\infty}^{+\infty} \cos[(\nu_{rf} + n)\theta + \chi] e^{i\kappa\theta} d\theta \tag{II.25}$$

$$= \frac{(1+G\gamma)}{2\pi} \frac{\int B_{rf} dl}{B\rho} \oint \frac{1}{2\pi} \sum_{n=-\infty}^{+\infty} \frac{e^{i(\nu_{rf}+n+\kappa)\theta + i\chi} + e^{-i(\nu_{rf}+n-\kappa)\theta - i\chi}}{2} d\theta. \tag{II.26}$$

Due to the periodic nature of the integrand in Eq. (II.26), the integral in Eq. (II.26) is non-zero only when the resonance tune κ is given by

$$\kappa = \pm(\nu_{rf} + n). \tag{II.27}$$

When the condition of Eq. (II.27) is satisfied, then Eq. (II.26) gives the following expression for the absolute value of the rf-dipole-induced spin resonance strength:

$$|\mathcal{E}_{Bdl}^{dip}| = \frac{1}{4\pi} \frac{e(1+G\gamma)}{p} \int B_{rf} dl. \tag{II.28}$$

Note that, as will be discussed later, there is now some question about the validity of Eq. (II.28).

Equation (II.27) determines the condition for an rf-induced spin resonance, which occurs when

$$\nu_s = \kappa = \pm(\nu_{rf} + n) \tag{II.29}$$

or

$$\nu_{rf} = k \pm \nu_s, \tag{II.30}$$

where n and k are arbitrary integers. Using the relations $\nu_{rf} = f_{rf}/f_c$ and $\nu_s = G\gamma$ in Eq. (II.30), one can obtain the frequency f_{rf}, at which an rf-induced spin resonance occurs

$$f_{rf} = f_c(k \pm G\gamma), \tag{II.31}$$

where f_c is the beam's circulation frequency, G is the particle's gyromagnetic anomaly, and γ is its Lorentz energy factor.

Similarly, for an rf solenoid with an oscillating longitudinal magnetic field

$$B_l(t) = B_{rf}\cos(2\pi f_{rf}t + \chi), \tag{II.32}$$

one can show that its rf-induced spin resonance strength is given by

$$|\varepsilon^{sol}_{Bdl}| = \frac{1}{4\pi}\frac{e(1+G)}{p}\int B_{rf}dl. \tag{II.33}$$

The resonance condition for an rf-induced spin resonance due to an rf solenoid is the same as for an rf dipole, i.e. Eq. (II.31).

II.2.3 Enhancement or Reduction of the RF-Induced Spin Resonance Strength

The rf-dipole-induced spin resonance strength in Eq. (II.28) was derived assuming that the rf dipole is the only source of the spin perturbation. However, this assumption is not completely realistic, because unlike an rf solenoid, an rf dipole not only perturbs the spin, but also affects the beam's orbital motion. A radial-field rf dipole excites forced vertical oscillations of the beam at the rf dipole's frequency, which drive the vertically polarized beam into the stronger radial field region of the ring's focusing quadrupoles [44, 47, 48]. These radial quadrupole fields experienced by the particles' spins may have a significant effect on the beam's polarization by making the rf-induced spin resonance weaker or stronger.

To be more quantitative, consider an isolated rf-induced spin resonance with its resonance tune κ defined as

$$\kappa \equiv f_r/f_c, \tag{II.34}$$

where f_r is the resonance frequency and f_c is the circulation frequency in the ring. As follows from the discussion above, the total resonance strength can be written as

$$\mathcal{E} = \mathcal{E}_{Bdl}^{dip} + \mathcal{E}_{fo}, \tag{II.35}$$

where $\mathcal{E}_{Bdl}^{dip}$ is the resonance strength given by Eq. (II.28) due to the rf dipole itself, and $\mathcal{E}_{fo}$ is the resonance strength contribution due to the forced oscillations inside the focusing quadrupoles. The forced contribution $\mathcal{E}_{fo}$ can be obtained from Eq. (II.18); it is given by [44]

$$\mathcal{E}_{fo} = \frac{(1+G\gamma)}{2\pi} \oint \frac{1}{B}\frac{\partial B_x}{\partial y}(\theta) y(\theta) e^{i\kappa\theta} d\theta, \tag{II.36}$$

where we used

$$\tilde{B_x}(\theta) = \frac{\partial B_x}{\partial y}(\theta) y(\theta). \tag{II.37}$$

The vertical beam displacement $y(\theta)$ due to the forced oscillations is given by [44]

$$y(\theta) = \frac{1}{4\pi|\nu_y - \nu_{rf} + k|} \int B_{rf} dl \frac{\sqrt{\beta_y(\theta)\beta_{dip}}}{B\rho} \cos[\nu_{rf}\phi_{rf}(\theta) + \chi], \tag{II.38}$$

where ν_y is the vertical betatron tune, $\nu_{rf} \equiv f_{rf}/f_c$ is the excitation tune, $\beta_y(\theta)$ is the vertical betatron function, β_{dip} is the betatron function's value at the rf dipole's location, $B\rho$ is the magnetic rigidity, and $\phi_{rf}(\theta)$ is the phase advance of the forced oscillations. Inserting Eq. (II.38) into Eq. (II.36) gives [44]

$$\begin{aligned} \mathcal{E}_{fo} \;\; = \;\; & \frac{(1+G\gamma)}{2\pi} \frac{\int B_{rf} dl}{4\pi|\nu_y - \nu_{rf} + k|} \times \\ & \oint \frac{\sqrt{\beta_y(\theta)\beta_{dip}}}{B^2\rho} \frac{\partial B_x}{\partial y}(\theta) \cos[\nu_{rf}\phi_{rf}(\theta) + \chi] e^{i\kappa\theta} d\theta. \end{aligned} \tag{II.39}$$

For the spin-flipping studies, we adjusted ν_{rf} to satisfy the condition $\kappa = k \pm \nu_{rf}$. Thus, the circular integral in Eq. (II.39) may be non-zero and there may be non-zero contribution to the rf-induced spin resonance strength caused by the forced oscillations. Note that the forced contribution $\mathcal{E}_{fo}$ in Eq. (II.39) is directly proportional to $\int B_{rf} dl$ and inversely proportional to the tune difference in the denominator $|\nu_y - \nu_{rf} + k|$. When ν_y is close to ν_{rf}, $\mathcal{E}_{fo}$ may become very large and thus greatly enhance the rf-induced resonance strength. Using Eqs. (II.28), (II.35), and (II.39), the dependence of the total rf-induced resonance strength $\mathcal{E}$ on the vertical betatron tune ν_y can be written as

$$\frac{\mathcal{E}}{\mathcal{E}_{Bdl}^{dip}} = 1 + \frac{C}{|\nu_y - \nu_{rf} + k|}, \tag{II.40}$$

where

$$C = \frac{1}{2\pi} \oint \frac{\sqrt{\beta_y(\theta)\beta_{dip}}}{B} \frac{\partial B_x}{\partial y}(\theta) \cos[\nu_{rf}\phi_{rf}(\theta) + \chi] e^{i\kappa\theta} d\theta \tag{II.41}$$

is a complex parameter, which is independent of ν_y to first order.

II.3 Froissart-Stora Equation and Spin-Flipping

In the previous section, we showed that the initially vertical polarization of a beam, which is stored in a flat circular accelerator with no special spin rotators, can be perturbed by a horizontal rf magnetic field from either an rf solenoid or an rf dipole. Moreover, this perturbation can induce an rf spin resonance when each particle's spin coherently encounters the horizontal magnetic field during each turn around the ring.

The spin's projection onto the vertical axis y is given by

$$S_y = \psi^\dagger \sigma_y \psi. \tag{II.42}$$

The beam's vertical polarization at some time t is the sum over all its particles' vertical spin components, divided by the number of particles

$$P_y = \frac{1}{N} \sum_{i=1}^{N} S_{yi}, \tag{II.43}$$

where S_{yi} is spin projection of particle i onto the y-axis.

In case of an isolated resonance, Eq. (II.13) becomes

$$\zeta(\theta) = \mathcal{E}_\kappa e^{-i\kappa\theta}. \tag{II.44}$$

Then Eq. (II.42) can be solved analytically for a constant-rate linear crossing of a resonance from $\theta = -\infty$ to $\theta = \infty$.

For an initial polarization $P_y(-\infty) = 1$, after the beam crosses the resonance, the polarization becomes

$$P_y(\infty) = 2e^{-\pi|\mathcal{E}|^2/2\Gamma} - 1, \tag{II.45}$$

where Γ is called the crossing rate, and $\mathcal{E}$ is the resonance strength. Eq. (II.45) was first derived by Froissart and Stora in 1960 [17].

This formula shows that if a resonance is very weak and/or it is crossed very quickly ($|\mathcal{E}|^2/\Gamma \ll 1$), then there is almost no loss of polarization. Moreover, when a resonance is very strong and/or it is crossed very slowly ($|\mathcal{E}|^2/\Gamma \gg 1$), then the polarization direction is flipped with almost no loss of polarization. A large polarization loss can occur when the crossing speed Γ is comparable to $|\mathcal{E}|^2$.

The resonance crossing rate Γ can be written as [17]

$$\Gamma = \frac{d}{d\theta}[\kappa - \nu_s] = \frac{1}{2\pi f_c}\frac{d}{dt}[\kappa - \nu_s], \tag{II.46}$$

where κ is the resonance tune, ν_s is the spin tune, and f_c is the circulation frequency. According to Eq. (II.46) a resonance crossing can occur when either the resonance

tune or the spin tune is changed. When a beam is accelerated, its spin tune $\nu_s = G\gamma$ changes as γ changes; thus, the beam may encounter many spin-depolarizing resonances during normal acceleration.

If one crosses a resonance by changing the resonance tune, then one can flip the polarization of the beam while keeping all other beam parameters unchanged. An appropriate spin resonance can be created in a ring by inserting either an rf solenoid with a longitudinal rf magnetic field [25, 27, 28] or an rf dipole with a transverse rf magnetic field [18, 19, 21, 22, 23, 24, 29, 30, 31]. Using this rf resonance to spin-flip a stored polarized beam can significantly reduce the systematic errors in a scattering experiment's spin asymmetry measurements.

One can define the spin flip efficiency as

$$\eta \equiv \frac{-P_f}{P_i}. \tag{II.47}$$

where P_f is the beam's final polarization, and P_i is the beam's initial polarization. When η is very close to 1, then one can spin-flip the beam many times with little loss of polarization.

CHAPTER III

EXPERIMENTAL APPARATUS

III.1 COoler SYnthrotron (COSY)

COSY is a COoler SYnchrotron and storage ring for medium energy physics, in Jülich, Germany. The cooler ring delivers protons and deuterons in the momentum range 270 to 3300 MeV/c. The COSY facility consists of an ion source, an injector cyclotron, a 100-m-long injection beam line, a 184-m-circumference ring and extraction beam lines. It has an electron cooling system that operates at injection, and a stochastic cooling system that operates at momenta between 1500 and 3300 MeV/c.

The apparatus used for our experiments is shown in Fig. III.1; it includes the polarized ion source [50, 51, 52], the injector cyclotron [53, 54, 55], the Low Energy Polarimeter (LEP) [56], which monitored the beam's polarization before injection into COSY, the COSY storage ring [57, 58, 59, 60], the electron Cooler [61], the EDDA detector [62, 63, 64, 65], and the rf dipole [66, 67] (or the rf solenoid [68, 69]).

III.1.1 Polarized Ion Source

The COSY polarized ion source was designed and built by a collaboration of groups from the universities of Bonn, Erlangen, and Cologne [50, 51, 52]. It produces negatively charged polarized beams of hydrogen H^- or deuterium D^-. A schematic view of the source is shown in Fig. III.2. It contains three main components: the atomic beam source that produces an intense polarized atomic hydrogen $\vec{H}^0$ or deuterium beam $\vec{D}^0$, the cesium beam source that produces a fast neutral Cs^0 beam, and the charge-exchange region where the $\vec{H}^0(\vec{D}^0)$ beam collides with the Cs^0 beam.

To produce an atomic beam, the H_2 or D_2 molecules were first dissociated in the 300-400 W rf dissociator. Then, the atoms passed through a 20-mm-long aluminum

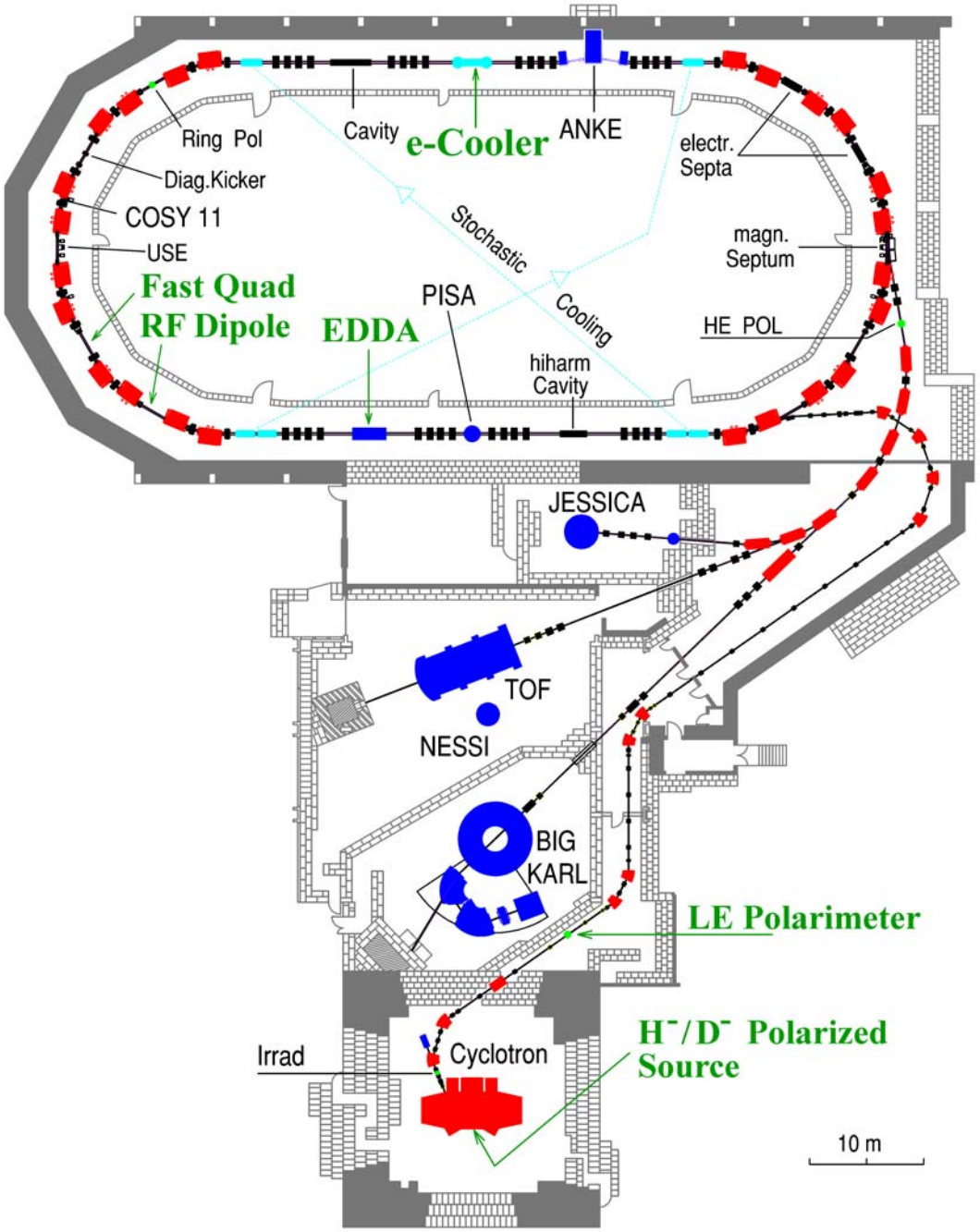

Figure III.1: Layout of the COSY accelerator facility showing the polarized ion source, the injector cyclotron, the Low Energy Polarimeter, and the COSY ring with its EDDA detector, electron Cooler, rf dipole, and fast quadrupole.

nozzle with a 3 mm diameter where they were cooled to about 30 K. This slowed the atoms allowing shorter sextupoles and increasing the acceptance solid angle; it also increased the ionization probability in the charge-exchange region by increasing the time atoms stayed there. Next, the atomic beam was polarized by passing through the two sextupoles and three rf transition units (RFT's).

In a strong magnetic field, the electron spin component m_e and the proton spin component m_p can be either $+\frac{1}{2}$ or $-\frac{1}{2}$, the deuteron spin component m_d can be -1, 0 or 1. Thus, the hydrogen (deuterium) atoms are split into four (six) hyperfine states, which are numbered in the order of decreasing of their energy. The hydrogen's hyperfine states $|m_p, m_e\rangle$ are:

$$|1\rangle = |+\tfrac{1}{2}, +\tfrac{1}{2}\rangle, \quad |2\rangle = |-\tfrac{1}{2}, +\tfrac{1}{2}\rangle, \quad |3\rangle = |-\tfrac{1}{2}, -\tfrac{1}{2}\rangle, \quad |4\rangle = |+\tfrac{1}{2}, -\tfrac{1}{2}\rangle.$$

The deuterium's hyperfine states $|m_d, m_e\rangle$ are:

$$|1\rangle = |+1, +\tfrac{1}{2}\rangle, \quad |2\rangle = |0, +\tfrac{1}{2}\rangle, \quad |3\rangle = |-1, +\tfrac{1}{2}\rangle,$$
$$|4\rangle = |-1, -\tfrac{1}{2}\rangle, \quad |5\rangle = |0, -\tfrac{1}{2}\rangle, \quad |6\rangle = |+1, -\tfrac{1}{2}\rangle.$$

In a weak magnetic field the electron and nuclear spins are coupled to each other. Thus, the spin state of an atom can not be described by one 'pure' spin state, but is instead a mixture of the states defined above. The sextupole magnets focus the states with $m_e = +\frac{1}{2}$ and defocus the states with $m_e = -\frac{1}{2}$. The RFT's operate at some magnetic field and frequency that drive rf-induced transitions, exchanging the populations of pairs of the hyperfine states. A set of three RFT's allows a large number of combinations.

The cesium (Cs) source is located opposite to the atomic $\vec{H}^0/\vec{D}^0$ beam source, as shown in Fig. III.2. First, the Cs vapor was thermally ionizes on a hot (1200 °C)

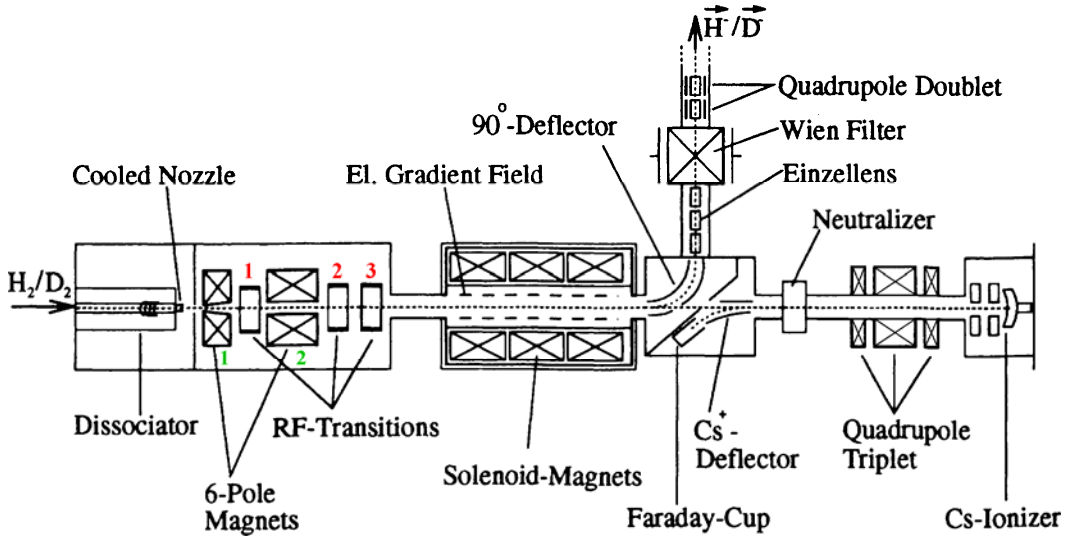

Figure III.2: Schematic view of the COSY's polarized ion source.

porous tungsten surface. Then, the Cs^+ ions were accelerated by a potential of 40-60 kV and focused by a triplet of magnetic quadrupoles. Next, the Cs^+ beam passed through a neutralizer filled with Cs^0 vapor, which neutralized the beam by capturing an electron. The neutral Cs beam entered the charge-exchange region through an orifice in the 90°-deflector. To avoid excessive Cs contamination of the source, the neutralizer was filled with Cs^0 vapor only during the short COSY injection pulses and was emptied between the pulses. Then the Cs^+ ions were no longer neutralized, and got deflected by the Cs^+ deflector into the Faraday cup.

In the charge exchange region the polarized atomic $\vec{H}^0(\vec{D}^0)$ beam collided with the fast neutral Cs^0 beam and exchanged electrons:

$$\vec{H}^0(\vec{D}^0) + Cs^0 \rightarrow \vec{H}^-(\vec{D}^-) + Cs^+.$$

An electric field inside the charge exchange region guided the negatively charged $\vec{H}^-(\vec{D}^-)$ atoms into the 90°-deflector that transfered them to the cyclotron. The atoms passed through the Wien Filter, which consists of perpendicular electric and magnetic fields that are perpendicular to the ion's trajectory. The electric and magnetic fields were adjusted so that the spin would be parallel to the magnetic field inside the cyclotron, and only ions with the correct velocity and mass-to-charge ratio could pass. The extracted beam current was about 20 μA for $\vec{H}^-$, and up to 16 μA for $\vec{D}^-$; the beam's typical vector polarization was about 80% for $\vec{H}^-$ and up to 70% for $\vec{D}^-$.

III.1.2 Injector Cyclotron

The cyclotron [53, 54, 55] delivered about 1 μA of polarized $\vec{H}^-$ ($\vec{D}^-$) ions at 45 MeV (75 MeV) for strip-injection into COSY. Its schematic layout, together with the ion source and its beam line, is shown in Fig. III.3. The cyclotron injected the ions into COSY in pulses lasting 10 to 20 ms at a maximum repetition rate of 0.5 Hz. Most cyclotron systems operated continuously, and the beam pulses were generated by a chopper in the source beam line (QBL). The H^- and D^- ion beams were injected into the cyclotron at 4.5 keV and 7.6 keV, respectively. The ion beam was matched to the rf-phase acceptance of the cyclotron by a buncher with a sinusoidal voltage, which is located below the cyclotron; it could also be combined with a special sawtooth buncher. A hyperbolic inflector (HI) near the center of the cyclotron was used for final injection onto a constant orbit.

The cyclotron has three spiral sector magnets (hills, shown in purple in Fig. III.3); the magnetic field was produced by a pair of main coils wound around each magnet's poles and a set of correction coils located on the pole faces. The magnetic field was stabilized to $\sim 10^{-6}$ using an NMR feedback system. Three Dees (shown in blue in

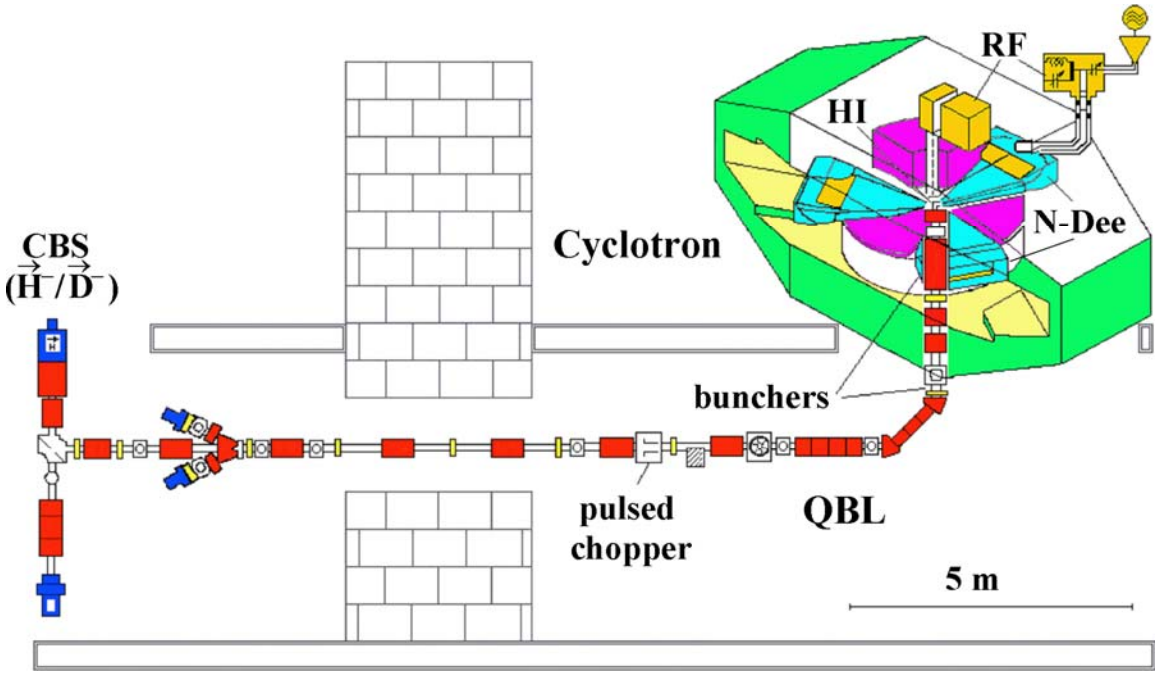

Figure III.3: Schematic view of the cyclotron with the colliding beams ion source (CBS) and the source beam line (QBL).

Fig. III.3) located between the hills provided the acceleration; they operate on the 3^{rd} harmonic of the orbital frequency, in the range of 20 to 30 MHz with a peak voltage of up to 40 kV. For acceleration of $\vec{H}^-$ ($\vec{D}^-$) ions to 45 MeV (75 MeV), one used a frequency of ∼29.6 MHz (∼27.3 MHz) and a voltage amplitude of ∼20 kV (∼33 kV). To keep the frequency in tune, the Dees were connected in the central region to a capacitively terminated resonance line. The beam was multi-turn extracted by a septum deflector, located in the pole gap of one of the hills.

III.1.3 COSY Ring

The COSY ring itself [57, 58, 59, 60] has a race-track geometry formed by two 52-m-long 180° arcs joined by two 40-m-long straight sections, adding up to a circumference of 184 m. A schematic view of the ring was shown in Fig. III.1. Each straight section contains four optical triplets (each consisting of four quadrupoles), designed to produce either a π or 2π betatron phase advance in each straight section. One straight section is used for two internal target experiments (COSY-13 and EDDA), the other provides space for the accelerating rf cavity, the electron cooler, scrapers, Schottky pickups, current monitors, and recently the WASA experiment.

Each of the two arc section consists of three almost identical cells. Each cell con-

tains 4 bending dipoles, 4 quadrupoles, and 1 or 2 sextupoles. Each half-cell has a FODO structure with the possibility of exchanging the focusing (F) and defocusing (D) for additional flexibility in adjusting the betatron tunes. The half-cells are arranged in a mirror-symmetric way, leading to a six-fold symmetry of the ring's magnetic lattice. One arc houses the injection and extraction hardware including a stripping target, the bumper magnets for injection, and the electrostatic and magnetic septa for extraction. The other arc provides space for a third internal target area (COSY-11), a diagnostic kicker, the ultra-slow extraction (USE) elements, a fast quadrupole, and an rf dipole or rf solenoid for spin manipulation.

The pickups and kickers for stochastic cooling are located at the intersections of the straight sections and arcs. In total 18 sextupoles are installed in the COSY ring, 5 in each arc for chromatic corrections, and 4 in each straight section for resonant extraction. The ring also contains 30 horizontal and vertical beam position monitors along with 40 correction dipoles for closed orbit corrections.

To avoid crossing the transition energy during acceleration, which could lead to significant beam loss in the strong-focusing COSY ring, the transition energy was shifted upward and always kept above the beam's instantaneous energy during acceleration by adjusting the ring's lattice. Thus, the transition point was never crossed. After reaching the flat-top energy: the rf voltage was adiabatically turned off; the beam was debunched; and the transition energy was moved back to its nominal value. The beam could then be rebunched, if needed, with nearly no intensity loss.

For the successful acceleration of a polarized proton beam, a number of proton spin resonances had to be properly handled. Five imperfection spin resonances and ten vertical intrinsic spin resonances exist in COSY's energy range; they are listed in Table III.1 and Table III.2, respectively. The beam's polarization was fully flipped at the crossing of each imperfection resonance. The polarization loss during each spin

$G_p\gamma$	2	3	4	5	6
p (MeV/c)	463.8	1258.7	1871.2	2442.6	2996.4

Table III.1: Imperfection resonances at COSY.

	$6-\nu_y$	$-1+\nu_y$	$7-\nu_y$	$0+\nu_y$	$8-\nu_y$	$1+\nu_y$	$9-\nu_y$	$2+\nu_y$	$10-\nu_y$	$3+\nu_y$
$G_p\gamma$	2.38	2.62	3.38	3.62	4.38	4.62	5.38	5.62	6.38	6.62
p (MeV/c)	819.2	999.9	1499.5	1645.8	2091.4	2228.4	2654.6	2787.5	3204.4	3335.1

Table III.2: Intrinsic resonances at COSY (resonance momenta are given for $\nu_y = 3.62$).

flip was reduced to less than 1%, by enhancing strength of each resonance using fast vertical correction dipoles to increase the beam's vertical betatron amplitude. The intrinsic resonances are weaker than the imperfection resonances and cannot produce full spin flip. The beam's polarization was preserved at the crossing of each intrinsic resonance by making a vertical betatron tune jump using a fast pulsed quadrupole magnet installed around a ceramic vacuum pipe. It jumped the vertical betatron tune ν_y by about $\Delta\nu_y = 0.06$ during 10 μs; this reduced the polarization loss to less than 5% for the strongest $G\gamma = 8 - \nu_y$ intrinsic resonance, and to less than 1% for all other intrinsic resonances. The slower fall-off time of ν_y after the jump was typically adjusted to 40 ms or less to avoid double crossing of a resonance. To optimize the distance between the intrinsic resonances, ν_y was typically kept fixed at 3.525 during acceleration. Polarization losses for all the $G\gamma = n \pm \nu_x$ coupling intrinsic spin resonances were eliminated by separating the horizontal and vertical betatron tunes by $|\nu_x - \nu_y| > 0.15$.

These techniques allowed acceleration of polarized protons up to COSY's maximum momentum with only a few percent polarization loss. The total beam loss caused by the correction dipoles and the fast quadrupole during acceleration was under 10%. There were no intrinsic spin resonances for deuterons in COSY's energy range when ν_y was kept around 3.6 during acceleration.

III.1.4 Electron Cooler

The electron cooler [61] was used to reduce the emittance and momentum spread of the proton or deuteron beam after injection into the COSY ring. Although the electron cooler could produce a 100 keV electron beam of 3 A, the $p_\uparrow$ ($d_\uparrow$) ion losses increase substantially at higher currents. The cooler was used at the COSY's $p_\uparrow$ ($d_\uparrow$) ion energy of 45 MeV (75 MeV), which corresponds to an electron beam energy of 20.66 keV. The optimal current for a typical 10 s cooling time was 170 mA (250 mA) for the $p_\uparrow$ ($d_\uparrow$) ion beam. The electron beam diameter was about 25 mm. The geometric length of the cooling section is 2 m, while its effective length is 1.5 m. Two toroid magnets, on either side, turned the electron beam into (out of) the $p_\uparrow$ ($d_\uparrow$) ion beam's path.

The transverse emittance was measured using the H^0 atoms that were formed in a small quantity inside the electron cooler. These neutral atoms were not affected by the magnetic fields, thus, they could be detected by wire chambers located behind the first ring's bending dipole, about 25 m downstream of the electron cooler. The width of a beam position monitor's sum signal from a longitudinal Schottky scan was used to measure the beam momentum spread $\Delta p/p$. The correction dipoles and

quadrupoles of the electron cooler were used to match the directions of the electron and proton beams, and to compensate for the influence of the cooler's magnets.

In a test with 2×10^9 protons in the COSY ring, the analysis showed that the initial $\Delta p/p$ of 10^{-3} was reduced by an order of magnitude, to 10^{-4}. The wire chambers' data showed a transverse phase space reduction from 25π mm mrad down to 0.5π mm mrad after 6 s of cooling. The proton and electron beam directions were matched to better than 0.3 mrad to achieve these results.

III.1.5 EDDA Detector

The Excitation function Data acquisition Designed for Analysis of phase shifts (EDDA) detector [62, 63, 64, 65] is shown in Fig. III.4. The detector consists of two cylindrical double layers covering the laboratory polar angle range $10° < \theta_{lab} < 72°$ and about 82% of the full 4π solid angle. The inner double layer contains 640 scintillating fibers each with a 2.5 mm diameter. They were helically wound around

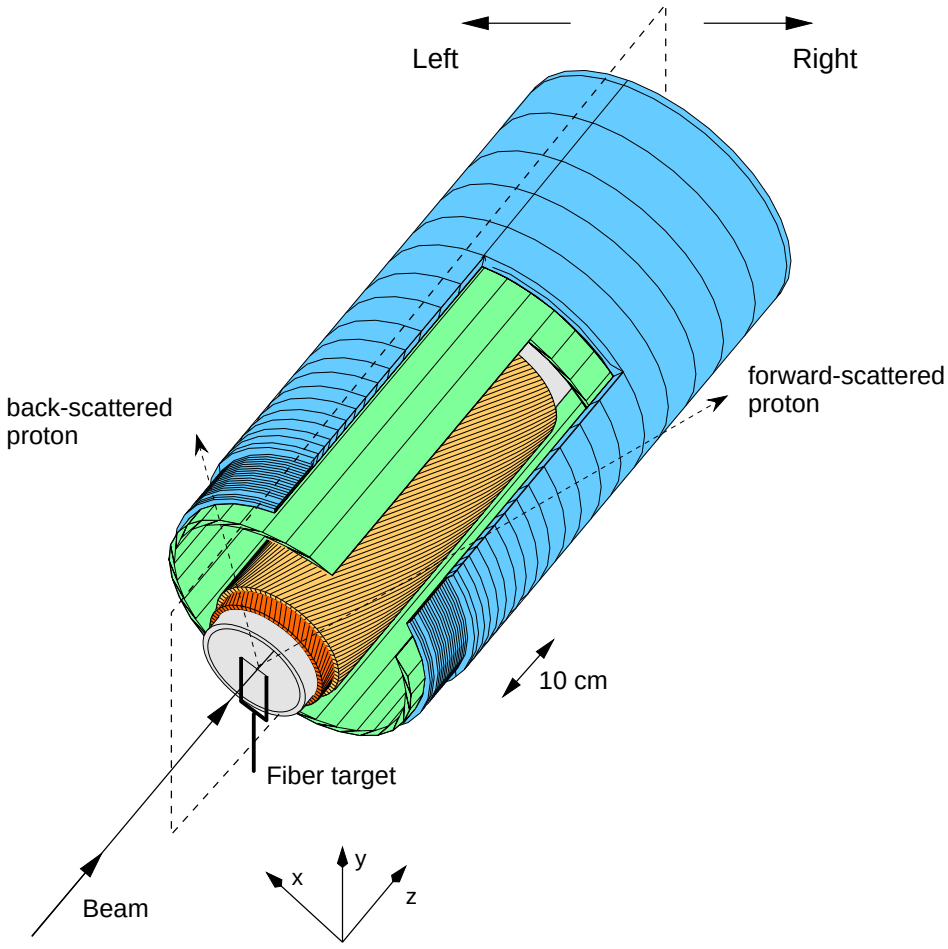

Figure III.4: The EDDA detector.

the beam pipe in two layers, with opposite helicities; the fibers are connected to 16-channel multi-anode photomultipliers. One of the outer double layers consists of 32 scintillator bars with triangular cross section, which are mounted parallel to the beam axis. Each bar spans an azimuthal angle of 11.25°. The second layer consists of 29 pairs of scintillator semi-rings, which surround the scintillator bars. The semi-rings close to the target are made from scintillating fibers. Each pair of the semi-rings covers θ_{lab} of about 2.5°. The scintillator cross sections were designed so that a particle passing through the outer double layer produces a position dependent signal in two neighboring bars and rings.

The resulting polar and azimuthal angular resolutions are about 1° and 1.9° FWHM, respectively. Combined with the spatial resolution of the inner layer's helical fibers, this allows one to do vertex reconstruction with a resolution of better than 2 mm in all dimensions. However, when taking exclusive *pp* elastic scattering data with EDDA, usable beam currents and detector count rates were greatly reduced due to the data acquisition dead time.

During our experiments EDDA was used as a very fast proton beam polarimeter. Background was suppressed by requiring a kinematic coincidence between the signals from the forward-scattered and back-scattered particles. EDDA counted only the trigger signals for the two-prong coincidence events in the left and right semi-rings. This method used only fast scalers and did not require any event reconstruction, thus, it had little dead-time and was very fast; further details can be found in [70]. The fast polarimeter was calibrated in a dedicated calibration run by measuring the effective analyzing power $A(p, \theta_{c.m.})$ of C fiber target. Exclusive *pp* elastic scattering data were taken simultaneously with fast scaler data. The effective analyzing power $A(p, \theta_{c.m.})$ was determined from

$$A(p, \theta_{c.m.}) = A_{pp}(p, \theta_{c.m.}) \frac{\alpha(p, \theta_{c.m.})}{\alpha_{pp}(p, \theta_{c.m.})}, \tag{III.1}$$

where $A_{pp}(p, \theta_{c.m.})$ is the analyzing power of *pp* elastic scattering, $\alpha(p, \theta_{c.m.})$ is the inclusive two-prong ring scaler asymmetry while $\alpha_{pp}(p, \theta_{c.m.})$ is the exclusive *pp* elastic scattering asymmetry.

We also used the EDDA detector to measure the deuteron polarization in COSY. EDDA was configured to operate as a very fast deuteron polarimeter by using scalers to count all particles scattered into the left (L), right (R), top (T), and bottom (B) quadrants of EDDA's outer scintillator double layer. The measured L, R, T, and B counts were used to form the vector $\alpha_{_V}$ and tensor $\alpha_{_T}$ scattering asymmetries:

$$\alpha_{_V} \equiv \frac{L - R}{L + R}, \tag{III.2}$$

$$\alpha_{_T} \equiv 4\frac{(L+R)-(T+B)}{L+R+T+B}. \tag{III.3}$$

The measured vector $\alpha_{_V}$ and tensor $\alpha_{_T}$ asymmetries are related to the beam's vector P_V and tensor P_T polarizations [71, 72, 73, 74] by the equations.

$$\alpha_{_V} = \frac{[1-\frac{\eta_{_R}}{\eta_{_L}}]+[1+\frac{\eta_{_R}}{\eta_{_L}}]\frac{3}{2}A'_yP_V+[1-\frac{\eta_{_R}}{\eta_{_L}}]\frac{1}{2}A'_{yy}P_T}{[1+\frac{\eta_{_R}}{\eta_{_L}}]+[1-\frac{\eta_{_R}}{\eta_{_L}}]\frac{3}{2}A'_yP_V+[1+\frac{\eta_{_R}}{\eta_{_L}}]\frac{1}{2}A'_{yy}P_T}, \tag{III.4}$$

$$\alpha_{_T} = 4\frac{[1+\frac{\eta_{_R}}{\eta_{_L}}-\frac{\eta_{_T}}{\eta_{_L}}-\frac{\eta_{_B}}{\eta_{_L}}]+[1-\frac{\eta_{_R}}{\eta_{_L}}]\frac{3}{2}A'_yP_V+}{[1+\frac{\eta_{_R}}{\eta_{_L}}+\frac{\eta_{_T}}{\eta_{_L}}+\frac{\eta_{_B}}{\eta_{_L}}]+[1-\frac{\eta_{_R}}{\eta_{_L}}]\frac{3}{2}A'_yP_V+} \frac{+[(1+\frac{\eta_{_R}}{\eta_{_L}})A'_{yy}-(\frac{\eta_{_T}}{\eta_{_L}}+\frac{\eta_{_B}}{\eta_{_L}})A'_{xx}]\frac{1}{2}P_T}{+[(1+\frac{\eta_{_R}}{\eta_{_L}})A'_{yy}+(\frac{\eta_{_T}}{\eta_{_L}}+\frac{\eta_{_B}}{\eta_{_L}})A'_{xx}]\frac{1}{2}P_T}, \tag{III.5}$$

where $\eta_{_L}$, $\eta_{_R}$, $\eta_{_T}$ and $\eta_{_B}$ are the detection efficiencies of the left, right, top and bottom quadrants, respectively. We found the detection efficiency ratios $\eta_{_R}/\eta_{_L}$, $[(\eta_{_T}/\eta_{_L})+(\eta_{_B}/\eta_{_L})]$ and the "effective" analyzing powers A'_y, A'_{xx}, A'_{yy} during a special calibration run with a full detector readout. Later we used these measured parameters listed in Table III.3 to determine the vector and tensor polarizations from the measured scaler asymmetries.

Parameter	Value
$\eta_{_R}/\eta_{_L}$	0.961 ± 0.001
$[(\eta_{_T}/\eta_{_L})+(\eta_{_B}/\eta_{_L})]$	2.1064 ± 0.0015
A'_y	0.0962 ± 0.0023
A'_{xx}	-0.2975 ± 0.0810
A'_{yy}	-0.2058 ± 0.0816
$\overline{\Delta A'^2_{xx}}$	0.00656863
$\overline{\Delta A'^2_{yy}}$	0.00665173
$\overline{\Delta A'_{xx}\Delta A'_{yy}}$	0.00660606

Table III.3: The detecting efficiency ratios and "effective" analyzing powers.

III.2 Ferrite RF Dipole

The spin rotation due to a transverse rf magnetic field of an rf dipole is almost independent of energy at high energies; while the spin rotation due to a longitudinal rf magnetic field of an rf solenoid gets smaller as the beam's energy increases because of the Lorentz contraction of an rf solenoid's $\int Bdl$. Thus, an rf dipole was installed in COSY to study the spin-flipping and spin manipulation of polarized protons and

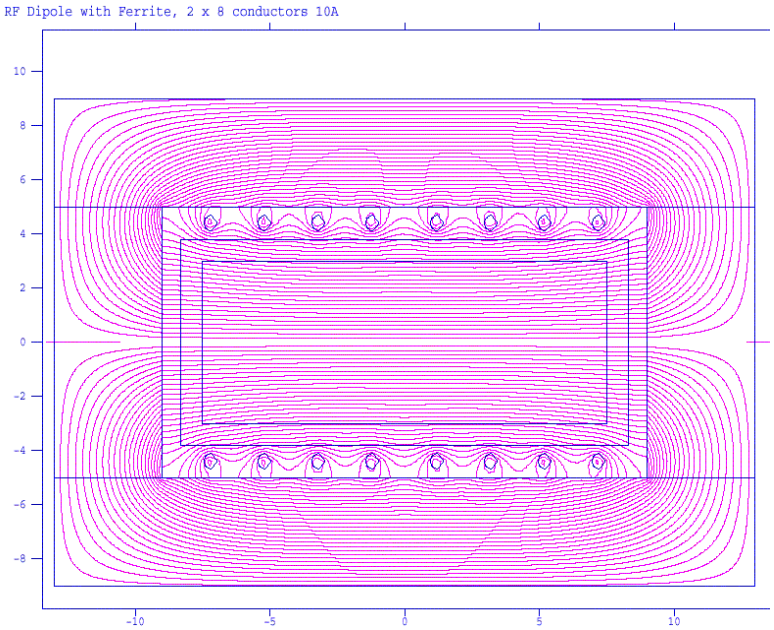

Figure III.5: Poisson-simulation of the rf dipole with a ferrite yoke.

deuterons. The rf dipole was designed at the University of Michigan [66] and built and tested at COSY [67]. The rf dipole's location in the ring is shown in Fig. III.1. It was installed around a ceramic vacuum pipe in place of the second fast quadrupole, which was no longer needed.

The dipole consists of an 8-turn copper coil surrounded by a ferrite yoke. The spacings between the coil's turns were optimized to produce a highly uniform radial

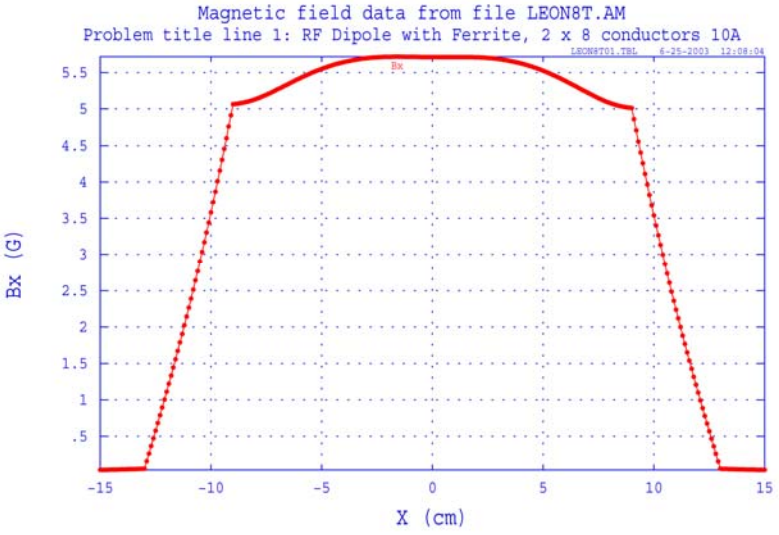

Figure III.6: RF dipole's transverse field B_x, calculated by the Poisson program for a nominal current of 10 A in the coil, plotted vs the radial coordinate.

magnetic field in the beam region, so that all particles in the beam would see the same $\int Bdl$; thus, their spins would all be rotated by the same amount. Fig. III.5 shows in red the B-field lines produced by a two-dimensional Poisson simulation for the rf dipole; the uniformity of the resulting transverse field is shown in Fig. III.6. Integrating from -350 mm to 350 mm with respect to the dipole's center gave a computed total field energy for a nominal current of 10 A in the coil, 1.41×10^{-3} Joule, giving an inductance of 28.2 μH and an $\int B_x dl$ of 0.3 T·mm. A three-dimensional MAFIA simulation of the rf dipole allowed calculating the integrals of all three magnetic field components along its axis.

$$\text{radial: } \int B_x dl/I = 0.03113 \text{ T·mm/A;} \tag{III.6}$$

$$\text{vertical: } \int B_y dl/I = 0.00012 \text{ T·mm/A;} \tag{III.7}$$

$$\text{longitudinal: } \int B_l dl/I = 0.00083 \text{ T·mm/A.} \tag{III.8}$$

Equations (III.6)-(III.8) clearly indicate that the vertical and longitudinal field components are small compared to the radial component. The calibration of Eq. (III.6)

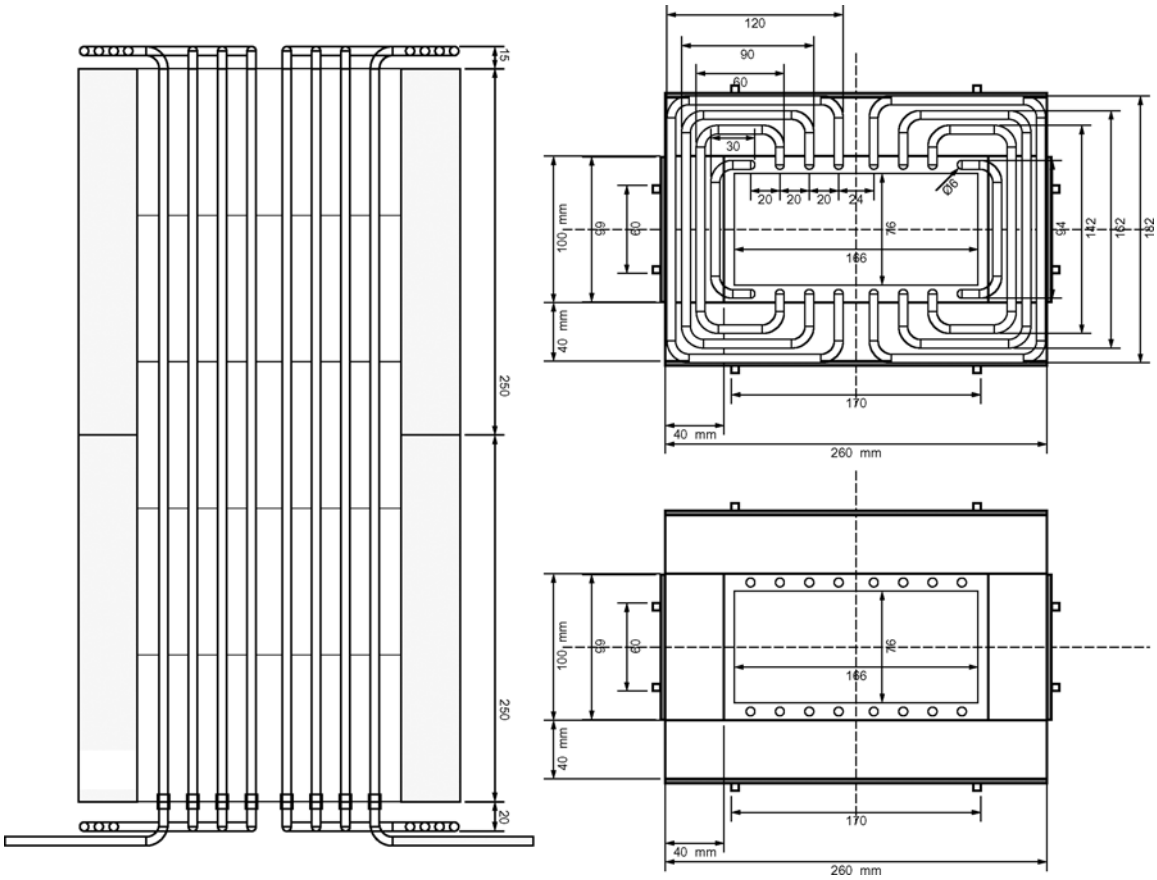

Figure III.7: RF dipole's design drawing showing the longitudinal cross section (left), front view (top right), and transverse cross section (bottom right).

was used to obtain the rf dipole's $\int B_x dl$ from its measured voltage V_{dipole}:

$$\int B_x dl = [\int B_x dl/I] \frac{V_{dipole}}{2\pi f_{rf} L}, \tag{III.9}$$

where $[\int B_x dl/I]$ is given by Eq. (III.6), f_{rf} is the rf dipole's frequency, and L is its inductance.

The coil was made of 6-mm-diameter copper tubing, which was cooled by the flow of water. A ferrite yoke was added to enhance the magnetic field's strength and improve its uniformity in the dipole's gap. The ferrite yoke was made of fourteen $265 \times 100 \times 40$ mm blocks of Ferroxcube 4L1 ferrite with a magnetic permeability of about $\mu = 240$. The ferrite yoke was cooled by water-cooled copper plates installed on its sides; with the normal water flow at 10 bar input pressure, the temperature rise was less than 10 degree. The rf dipole's construction drawing is shown in Fig. III.7. The photograph of the rf dipole installed in the COSY ring is shown in Fig. III.8.

To increase the rf dipole's magnetic field strength, it was a part of the LC resonant circuit shown in Fig. III.9. The variable capacitor C_p, with a range of 50 to 5000 pF, was connected in parallel with the dipole to form the resonant circuit. Its capacitance was adjusted to give the appropriate resonant frequency $f_r = (2\pi)^{-1}(LC)^{-1/2}$. The variable vacuum capacitor C_m, with a range of 5 to 500 pF, was wired in series with the LC resonant circuit to match the circuit's impedance to the 50 Ohm output impedance of the power supply.

The rf dipole's circuit was driven with up to 1 kW of input power produced by

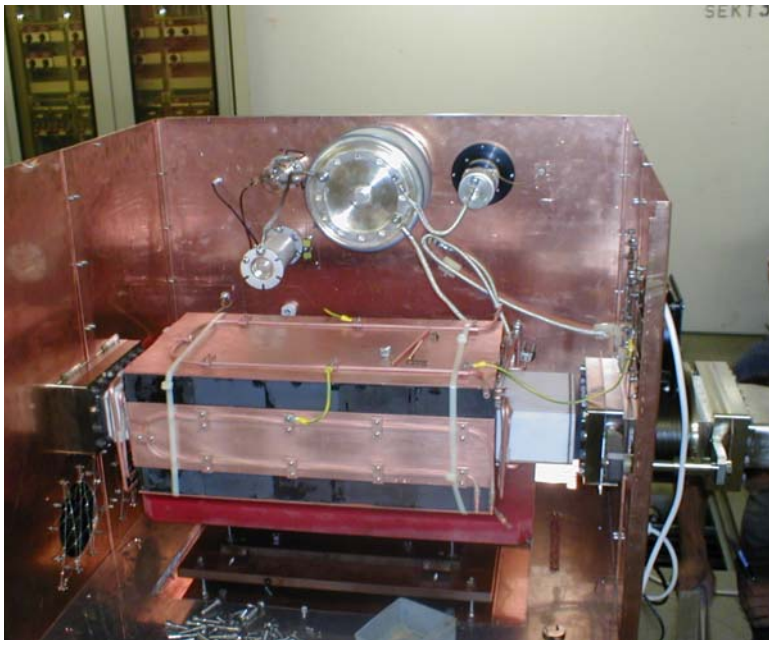

Figure III.8: RF dipole installed around a ceramic vacuum pipe in the COSY ring.

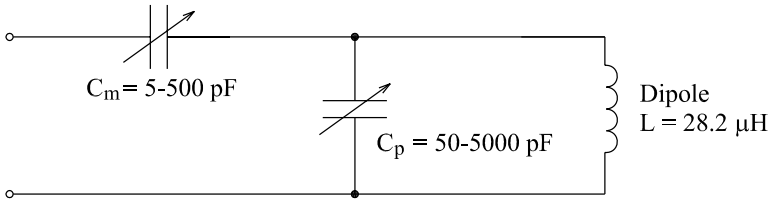

Figure III.9: RF dipole's resonant circuit.

combining the outputs of two ENI 500 W rf amplifiers. With 1 kW of forward power at 916 kHz, the rms voltage measured across the rf dipole was about 2.8 kV, which corresponded to an $\int B_{rms} dl$ of about 0.54 T·mm. The rf dipole's amplitude and frequency ramps were produced using a computer control system that was originally developed for COSY's ultra-slow extraction (USE) system. The timing of the control system was synchronized with COSY's operation to produce the proper amplitude and frequency ramps at the appropriate times during the accelerator cycle.

III.3 RF Solenoid

An rf solenoid magnet was later designed at the University of Michigan [68] and built and tested at COSY [69]. Poisson-simulations for the rf solenoid and its resulting longitudinal field are shown in Figs. III.10 and III.11. The simulation gave an inductance of about 40 μH and an $\int Bdl$ of 0.67 T·mm. To provide a site and rf power for the new rf solenoid, the COSY-Michigan ferrite rf dipole was disassembled

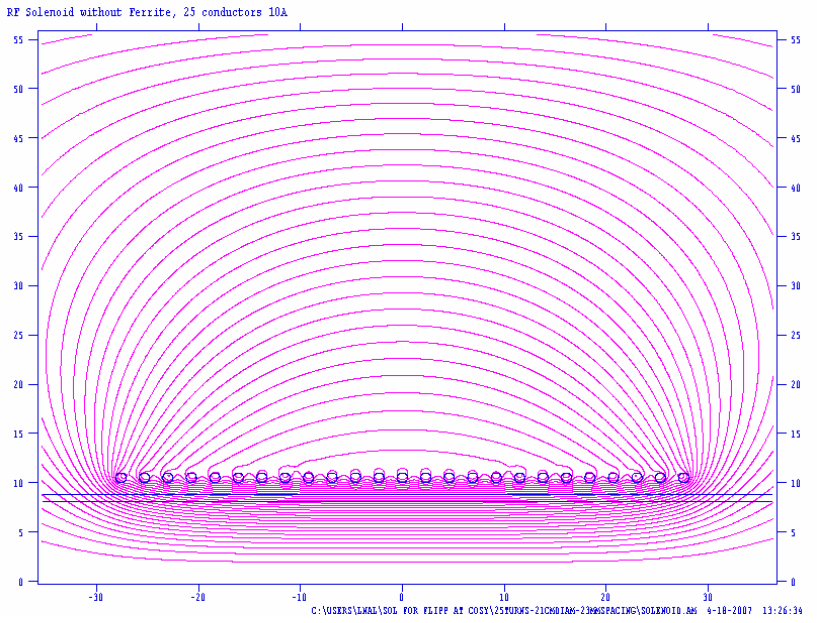

Figure III.10: Poisson-simulation of the rf solenoid.

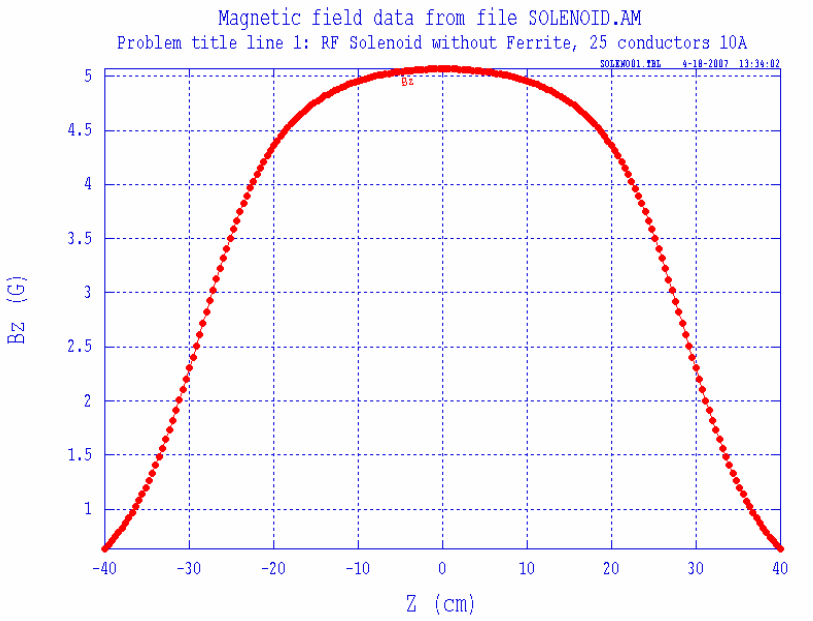

Figure III.11: RF solenoid's longitudinal field, calculated by the Poisson program for a nominal current of 10 A in the coil, plotted vs the longitudinal coordinate.

and stored, it can later be reinstalled in the COSY ring. The solenoid was installed around a ceramic vacuum pipe in place of the rf dipole.

The solenoid was a 57.5 cm-long 25-turn air-core copper coil with an average diameter of 21 cm as shown in Fig. III.12. The coil was made of the same type of 6-mm-diameter copper tubing as the rf dipole; thus, it was easily connected to the rf-dipole's water-cooling system. The rf solenoid's inductance and $\int Bdl$ are similar to those of the rf dipole; thus, it could easily use the rf dipole's resonant circuit and power supply system.

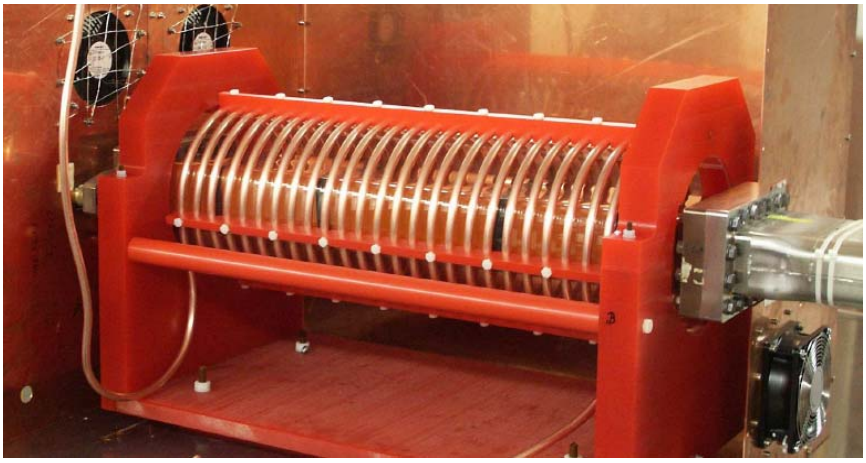

Figure III.12: RF solenoid installed around a ceramic vacuum pipe in the COSY ring.

Several pick-up loops were installed on the inside of the rf solenoid coil, to measure the solenoid's field just outside the ceramic vacuum pipe. The pick-up loops were 0.85-mm diameter wires wound one turn around a 24 mm diameter rod. For the loop at the solenoid's longitudinal center, at a frequency of 917 kHz, a peak-to-peak voltage of 4.75 V was measured on a monitor in the COSY control room. The wires of this pick-up loop were connected to the monitor part of the rf solenoid's circuit. The circuit diagram of rf solenoid's circuit, including the monitor is shown in Fig. III.13. This measured 4.75 V peak-to-peak voltage corresponds to a 3.26 V rms voltage across the pick-up loop. This gave an rf magnetic field at the solenoid's center of $B_{rms} = V/(2\pi f_r A) = 1.17 \times 10^{-3}$ T rms, or an $\int Bdl$ of 0.66 T·mm, which agrees with the simulation value very well.

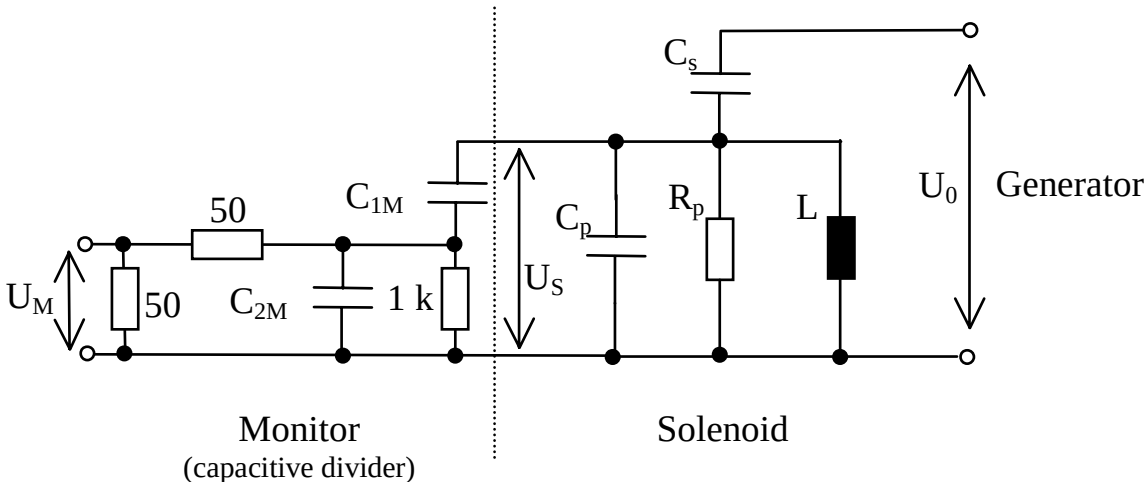

Figure III.13: RF solenoid's resonant circuit, including the monitor part located in the COSY control room.

CHAPTER IV

HIGHLY EFFICIENT SPIN FLIPPING OF POLARIZED PROTON BEAM AT COSY

An rf dipole was earlier used to spin flip 120 MeV (490 MeV/c) polarized protons stored in the IUCF Cooler Ring with a $99.93 \pm 0.02\%$ spin-flip efficiency. Due to the Lorentz invariance of an rf dipole magnet's transverse $\int Bdl$, and the resulting very weak energy dependence of its rf-induced spin-resonance strength, at very high energies an rf dipole's spin rotation angle should become almost independent of energy. Thus, a moderately strong small rf dipole should allow spin-flipping with more than 99.9% efficiency for protons in high energy rings, such as the 250 GeV Relativistic Hadron Collider, or even the 7 TeV Large Hadron Collider. To help confirm this, we conducted an experiment on the spin flipping of a 2.1 GeV/c vertically polarized proton beam stored in the COSY ring, which is described in this chapter.

IV.1 Introduction

The unperturbed spin motion of a particle beam in an ideal flat and circular storage ring or accelerator is a simple precession of each particle's spin vector around the vertical magnetic fields of the ring's bending dipoles. The spin tune, which is a number of spin precessions during one turn around the ring, is proportional to particle's energy and is given by

$$\nu_s = G\gamma, \tag{IV.1}$$

where G is particle's gyromagnetic anomaly (for protons $G_p = 1.792847$) and γ is its Lorentz factor. Any horizontal magnetic field would perturb this simple motion; and when the frequency of a horizontal-field rf magnet is correlated with the spin precession frequency, then an rf spin-depolarizing resonance is created at

$$f_r = f_c(k \pm \nu_s), \tag{IV.2}$$

where f_c is the particle's circulation frequency and k is an integer.

Adiabatically ramping the rf magnet's frequency through f_r can flip each proton's spin. The empirically modified [27, 31] Froissart-Stora equation [17] relates the beam's final polarization P_f to its initial polarization P_i after crossing the resonance,

$$P_f = P_i \left\{ (1+\hat{\eta}) \exp\left[\frac{-(\pi\, \varepsilon_{FS}\, f_c)^2}{\Delta f/\Delta t} \right] - \hat{\eta} \right\}. \tag{IV.3}$$

The limiting spin-flip efficiency $\hat{\eta}$ includes only losses due to mechanisms other than crossing the resonance being considered, while the measured spin-flip efficiency

$$\eta \equiv \frac{-P_f}{P_i}. \tag{IV.4}$$

also includes losses due to the resonance crossing. We maximized η by varying both Δf and Δt in the resonance crossing rate $\Delta f/\Delta t$, where Δf is the rf magnet's total frequency ramp range and Δt is its frequency ramp time. The rf-induced resonance strength ε_{FS} is proportional to the rf dipole's rms magnetic field integral $\int B_{rms} dl$, which was widely believed [36, 41, 43, 45] to be given by

$$\varepsilon_{Bdl} = \frac{1}{2\sqrt{2}\pi} \frac{e(1+G\gamma)}{p} \int B_{rms} dl, \tag{IV.5}$$

where e is the proton's charge and p is its momentum. Note, however, that Eq. (IV.5) is for an ideal flat circular accelerator with a point rf dipole causing the only perturbation of the spin motion, which is not realistic for most rings.

IV.2 Experimental Procedure and Analysis

We used the ferrite-yoke rf dipole, described in section III.2.1, with radial rf magnetic field to manipulate the beam's vertical polarization. The stored 2.1 GeV/c protons' measured circulation frequency in COSY was $f_c = 1.491\,892$ MHz, corresponding to a Lorentz energy factor γ of about 2.4514; with this γ, Eq. (IV.1) gave a spin tune $\nu_s = G\gamma$ near 4.3950. Thus, Eq. (IV.2) implies that the $k = 5$ rf spin-depolarizing resonance should be centered near

$$f_r = (5 - G\gamma) f_c = 902.62 \text{ kHz}. \tag{IV.6}$$

The proton beam emerging from the polarized H^- ion source was accelerated by the Cyclotron to COSY's 45 MeV injection energy. To monitor the stable operation and polarization of the ion source, the Low Energy Polarimeter measured the beam's vertical polarization at 45 MeV in the injection line, before injection into the COSY ring. During injection into COSY, acceleration and then storage at 2.1 GeV/c, the

horizontal and vertical betatron tunes were fixed at $\nu_x = 3.525$ and $\nu_y = 3.575$, respectively. The rf acceleration cavity was turned off and shorted during COSY's flat-top, thus, there were no synchrotron oscillations or sideband spin resonances. The EDDA detector measured the beam's vertical polarization in the COSY ring; we reduced its systematic errors by cycling the polarized source between the up and down vertical polarization states on alternate pulses. The measured proton polarization in COSY, before spin manipulation, was about 80%.

The rf dipole was a part of an LC resonant circuit, which operated near the circuit's resonance frequency of about 902.6 kHz at an rf voltage of 2.4 kV rms, giving an $\int B_{rms} dl$ of 0.46 ± 0.03 Tmm. Thus, Eq. (IV.5) gave an rf-induced spin resonance strength of $\varepsilon_{Bdl} = (40 \pm 3) \times 10^{-6}$.

IV.2.1 The Spin Resonance Search

In order to flip a stored beam's polarization with high efficiency using an rf-induced spin resonance, the resonance's exact location and width was first determined. Then the central frequency of the ramp was set to the resonance's central frequency f_r, and the ramp's frequency range Δf was chosen to completely cover the resonance width.

We first roughly measured this resonance's frequency by linearly ramping the rf-dipole's frequency around the f_r calculated in Eq. (IV.6); we first ramped it from $f_r - \Delta f/2$ to $f_r + \Delta f/2$ with $\Delta f/2 = 2$ kHz, while the ramp time was Δt set at 10 s. We then continued making these ± 2 kHz ramps, next to each side of the previous frequency range, until the beam was either spin-flipped or depolarized, as shown in Fig. IV.1. The ± 2 kHz ramps with no depolarization did not cross the rf-induced resonance; the ± 2 kHz ramps with depolarization or a partial spin-flip did cross some part of the resonance, and the ± 2 kHz ramps with an almost full spin-flip crossed almost the whole rf-induced resonance. The data's behavior and our previous experience [23] suggested that the resonance width was comparable to the ± 2 kHz frequency ramps.

Thus, we next repeated this experiment while first narrowing frequency ramps to $\Delta f/2 = 1$ kHz, and then finally to $\Delta f/2 = 0.2$ kHz, to better determine the resonance's exact location and width; these data are also shown in Fig. IV.1. Fitting the ± 0.2 kHz data to the indicated first-order Lorentzian curve gave a central resonance frequency of $f_r = 902.4 \pm 0.1$ kHz and a resonance width $w = 2.4 \pm 0.3$ kHz FWHM.

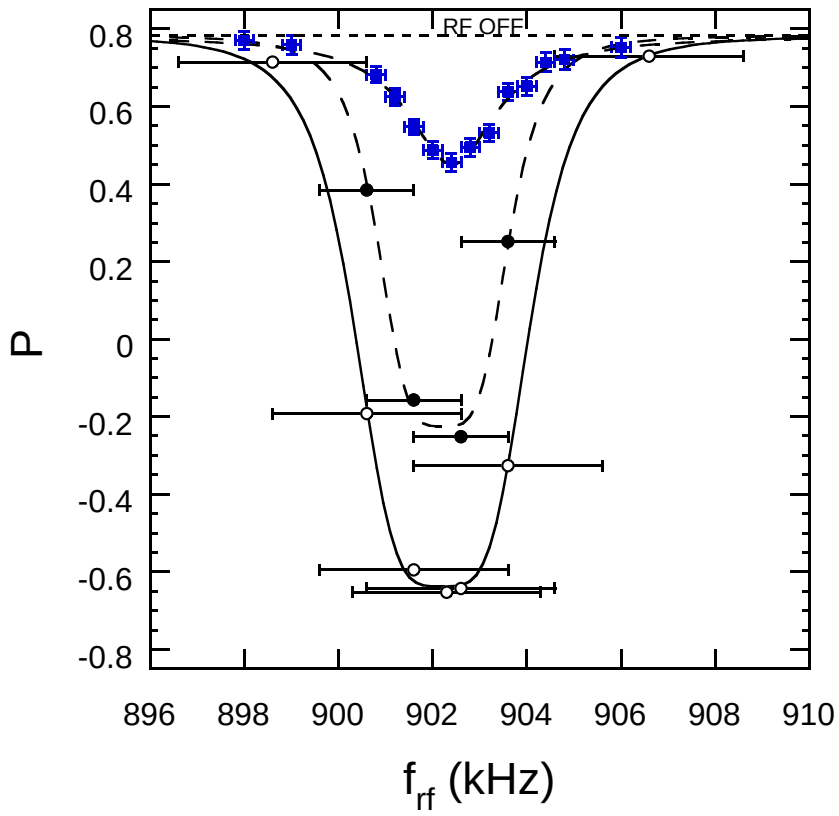

Figure IV.1: The measured proton polarization is plotted against the central frequency of each ramp; each ramp's frequency range Δf is shown by a horizontal bar; the ramp time Δt was set at 10 s. The curves are fits using 1^{st}-order Lorentzian for ± 0.2 kHz sweeps and 2^{nd}-order Lorentzians for ± 1 and ± 2 kHz sweeps. The ± 0.2 kHz data's fit gave $f_r = 902.4 \pm 0.1$ kHz and $w = 2.4 \pm 0.3$ kHz FWHM.

IV.2.2 Optimization of the Resonance Crossing Rate

To maximize the spin-flip efficiency, we varied the rf-dipole's frequency ramp's range Δf and ramp time Δt at the maximum $\int B_{rms} dl$. The frequency range Δf was centered at the $f_r = 902.4$ kHz measured in Fig. IV.1. We first spin-flipped the proton beam by ramping the rf-dipole's frequency through f_r with a constant frequency half-range $\Delta f/2 = 4$ kHz at various ramp times Δt, while measuring the final beam polarization after each ramp. We observed an almost full spin-flip at Δt of 0.007 s, as shown in Fig. IV.2. To ensure very efficient spin-flipping, we set Δt at 0.4 s, which was safely on the high-efficiency plateau and allowed us to proceed with our program quickly. The fit of Fig. IV.2 data to Eq.(IV.3) gave a limiting spin-flip efficiency of $\hat{\eta} = 98 \pm 1\%$.

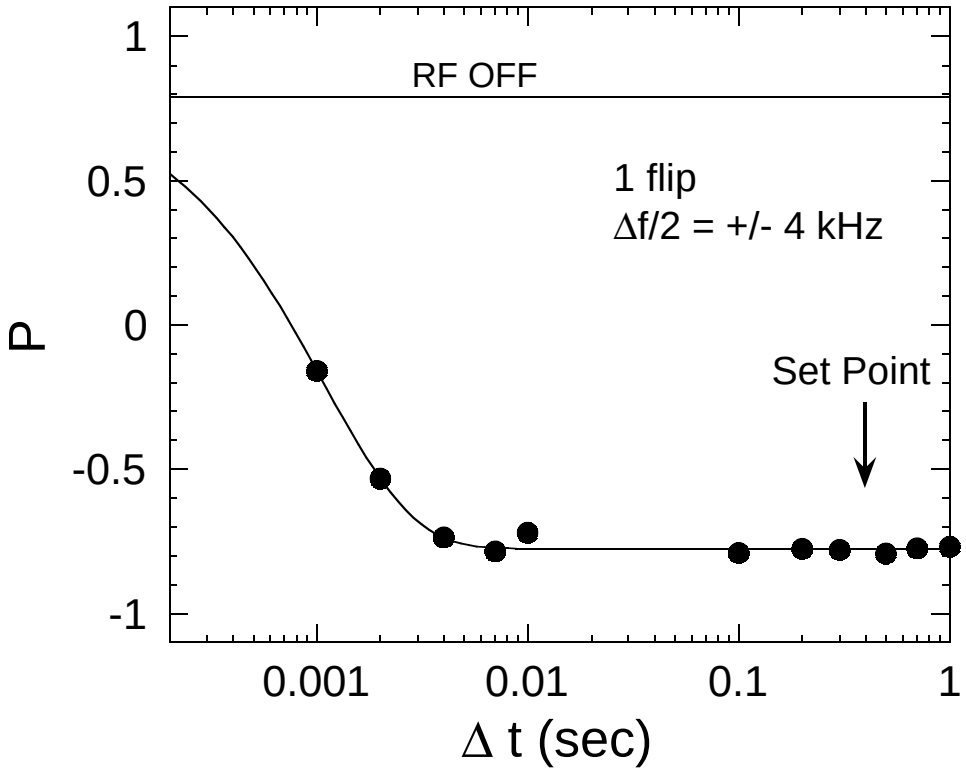

Figure IV.2: The proton final polarization measured after 1 spin-flip, is plotted against the rf-dipole's ramp time Δt. The curve is a fit to Eq. (IV.3), giving a limiting spin-flip efficiency of $\hat{\eta} = 98 \pm 1\%$. The arrow indicates the Δt chosen for the next study.

To find the optimum values for the rf-dipole frequency ramp parameters, we next measured the polarization after 11 spin-flips, while first varying the rf-dipole's frequency range Δf, and later its ramp time Δt, at the maximum $\int B_{rms} dl$. This multiple spin-flip technique enhanced small changes in the final beam polarization's dependence on the ramp parameters, because the 11^{th} power of even a small single spin-flip depolarization can be significant. We then obtained the single spin-flip efficiency for each data point from

$$\eta = \sqrt[11]{-P_{11}/P_i}, \tag{IV.7}$$

where P_{11} is the measured polarization after 11 spin-flips and P_i is the initial polarization. The measured polarization after 11 spin-flips and the single spin-flip efficiency are plotted against the rf-dipole's frequency half-range $\Delta f/2$ in Fig. IV.3; they showed no dependence on $\Delta f/2$ in the region of about 3 to 10 kHz. Thus, we set $\Delta f/2 = 6$ kHz to safely cover the resonance.

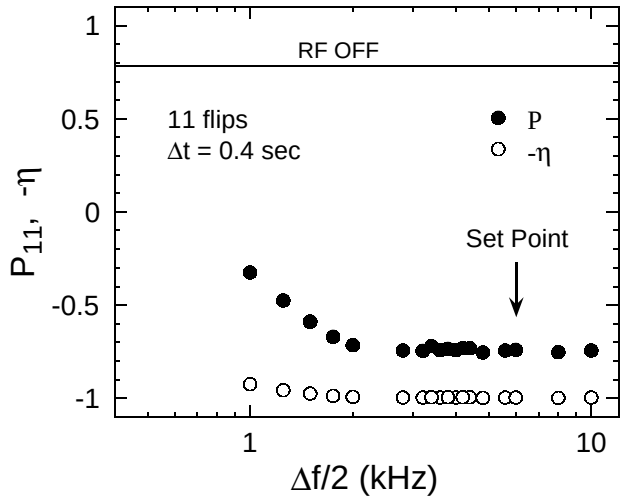

Figure IV.3: The final proton polarization measured after 11 spin-flips P_{11} and the spin-flip efficiency η calculated using Eq. (IV.7), are plotted against the rf-dipole's frequency half-range $\Delta f/2$. The arrow indicates the $\Delta f/2$ chosen for further studies.

We next measured the polarization after 11 spin-flips, P_{11}, while varying the rf-dipole's frequency ramp time Δt. Both the measured P_{11} and η are plotted against Δt in Fig. IV.4; using these data we set Δt at 0.1 s, where the spin-flip efficiency was high, while Δt was small enough to allow 51 spin flips fairly quickly. The fit of Fig. IV.4 data to Eq. (IV.3) gave a limiting spin-flip efficiency of $\hat{\eta} = 99 \pm 1\%$.

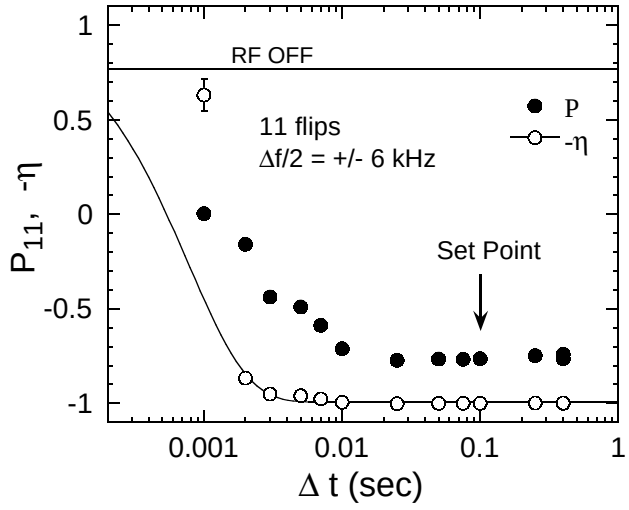

Figure IV.4: The final proton polarization measured after 11 spin-flips P_{11} and the spin-flip efficiency η calculated using Eq. (IV.7), are plotted against the rf-dipole's ramp time Δt. The curve is a fit to Eq. (IV.3), giving a limiting spin-flip efficiency of $\hat{\eta} = 99 \pm 1\%$. The arrow indicates the Δt chosen for further studies.

IV.2.3 Multiple Spin-Flipping

After setting Δt and Δf to maximize the spin-flip efficiency, we determined it much more precisely by measuring the final polarization while varying the number of spin-flips, up to 51, with Δt, Δf, and $\int Bdl$ all fixed at their optimum values. These data are plotted against the number of spin-flips in Fig. IV.5. We obtained the spin-flip efficiency η by fitting these data to

$$P_n = P_i \cdot (-\eta)^n, \tag{IV.8}$$

where P_n is the measured polarization after n spin-flips. The fit gave a measured spin-flip efficiency of $\eta = 99.92 \pm 0.04\%$.

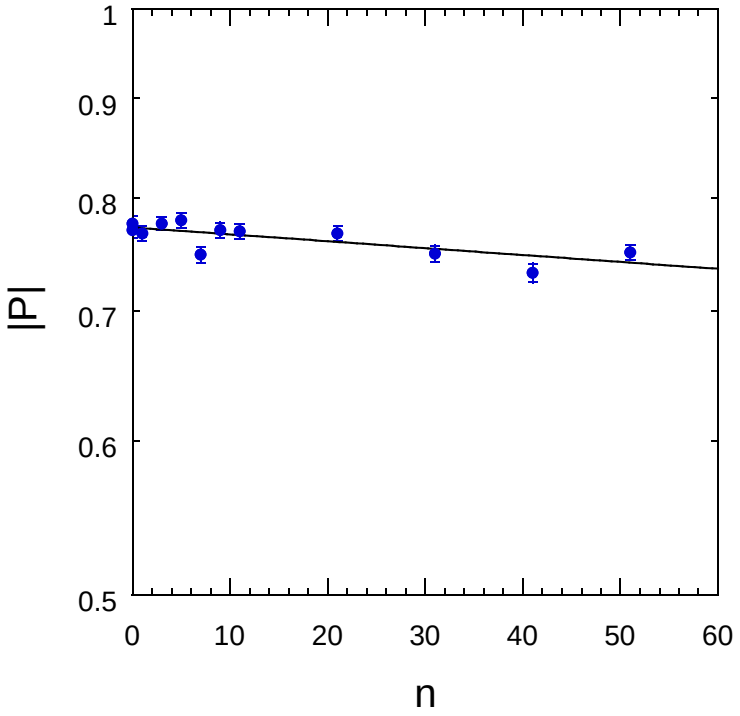

Figure IV.5: The magnitude of the measured proton polarization is plotted against the number of spin-flips. The rf-dipole's frequency ramp time Δt was 0.1 s; its frequency half-range $\Delta f/2$ was 6 kHz; and its $\int B_{rms} dl$ was 0.46 ± 0.03 T·mm. The line is a fit using Eq. (IV.8), giving a measured spin-flip efficiency of $\eta = 99.92 \pm 0.04\%$.

CHAPTER V

STRENGTH OF THE INDUCED SPIN RESONANCE

We earlier analyzed all available data on spin-flipping stored beams of polarized protons, electrons and deuterons [33]. Fits to the modified Froissart-Stora equation of the measured polarization data after crossing an rf-induced spin resonance, gave a spin resonance strength ε that deviated by factors of up to 10-20 in both directions from the strength given by the equations used for many years [36, 39, 41, 42, 43, 44, 45, 46]. The polarization was typically manipulated by linearly sweeping the frequency of an rf dipole or rf solenoid through an rf-induced spin resonance. Understanding such a disagreement is important for the correct estimation of the rf magnet's strength required for efficient spin flipping and other spin manipulations in storage rings. Therefore, we recently studied the resonance strength deviations experimentally using a 2.1 GeV/c polarized proton beam stored in COSY with an rf dipole, and using a 1.85 GeV/c polarized deuteron beam stored in COSY with both an rf dipole and an rf solenoid.

V.1 Overview of the Existing Spin-Flipping Data

The rf-induced spin resonance strength ε_{FS} was obtained experimentally by measuring the final beam polarization P_f after ramping an rf magnet's frequency through a spin resonance frequency f_r by a range Δf during different times Δt. Then P_f was plotted vs. the different Δt values and the data were fit to either the Froissart-Stora equation [17], Eq. (I.4), or to a modified [27, 31] Froissart-Stora equation, Eq. (IV.3), with ε_{FS} as a fit parameter.

It was widely believed [36, 39, 42, 43, 45, 46] that one could obtain the strength ε_{Bdl} of an rf-magnet-induced resonance using the equations

$$\text{Solenoid:} \qquad \varepsilon_{Bdl} = \frac{1}{2\sqrt{2}\pi} \frac{e(1+G)}{p} \int B_{rms} dl, \tag{V.1}$$

$$\text{Dipole:} \qquad \varepsilon_{Bdl} = \frac{1}{2\sqrt{2\pi}} \frac{e(1+G\gamma)}{p} \int B_{rms} dl, \tag{V.2}$$

where e is the particle's charge, p is its momentum, and $\int B_{rms} dl$ is the rf magnet's rms magnetic field integral in the particle's rest frame. These equations, however, were derived for a flat circular accelerator with a point rf magnet causing the only perturbation of the spin motion. This may not be a realistic assumption, especially for the transverse magnetic field of an rf dipole.

V.1.1 Compilation of Existing Data

We examined all available publications and logbooks for spin-flipping data [33] that allowed us to simultaneously obtain both: the spin resonance strength ε_{Bdl} from the rf magnet's $\int Bdl$, and the spin resonance strength ε_{FS} from polarization vs. ramp time Δt measurements. We also checked, in each experiment, for any other spin resonances near the rf-induced resonance. Fits to Eq. (IV.3), the modified Froissart-Stora equation, gave the measured spin resonance strength ε_{FS} for each experiment and its error. We also calculated the spin resonance strength from each rf magnet's $\int Bdl$ using Eq. (V.1) or (V.2). For the experiments at IUCF and MIT, there were no precise measurements of the rf magnet's $\int Bdl$; thus, we assumed a $\pm 10\%$ error. For the more recent experiments at COSY, the rf dipole's $\int Bdl$ was known with a $\pm 5\%$ uncertainty.

Then we took the ratio of the two spin resonance strengths, $\varepsilon_{FS}/\varepsilon_{Bdl}$, for each experiment and obtained its error using simple error propagation formulae. Figure V.1 from Ref. [33] shows these ratios obtained for protons and deuterons at IUCF and COSY and electrons at MIT plotted vs. the frequency range Δf used for each Δt curve.

This compilation indicated that for many experiments ε_{Bdl} and ε_{FS} disagree with the predictions [36, 42, 43, 45] by factors of 0.1, 10, or more. For the proton experiment described in Chapter IV, the ε_{Bdl} from Eq. (V.2) was $(40 \pm 3) \times 10^{-6}$, while the ε_{FS} obtained from Fig. IV.2 was $(580 \pm 10) \times 10^{-6}$, which is about 14.5 times larger. For the deuteron experiment, done with the same rf dipole at COSY and described later in this Chapter, ε_{Bdl} was $(7.9 \pm 0.5) \times 10^{-6}$, while ε_{FS} was $(1.17 \pm 0.01) \times 10^{-6}$, which is about 6.8 times smaller. Thus, these large deviations in opposite directions seemed unlikely to be due to an incorrect calibration of $\int Bdl$.

Figure V.1 showed that all data with small Δf had $\varepsilon_{FS}/\varepsilon_{Bdl}$ values far below 1, while all data with large Δf have $\varepsilon_{FS}/\varepsilon_{Bdl}$ values near or above 1. For deuterons, all $\varepsilon_{FS}/\varepsilon_{Bdl}$ ratios were far below 1 for rf dipoles, but closer to 1 for rf solenoids. This suggested some anomalous behavior of spin-1 deuterons when spin-manipulated by

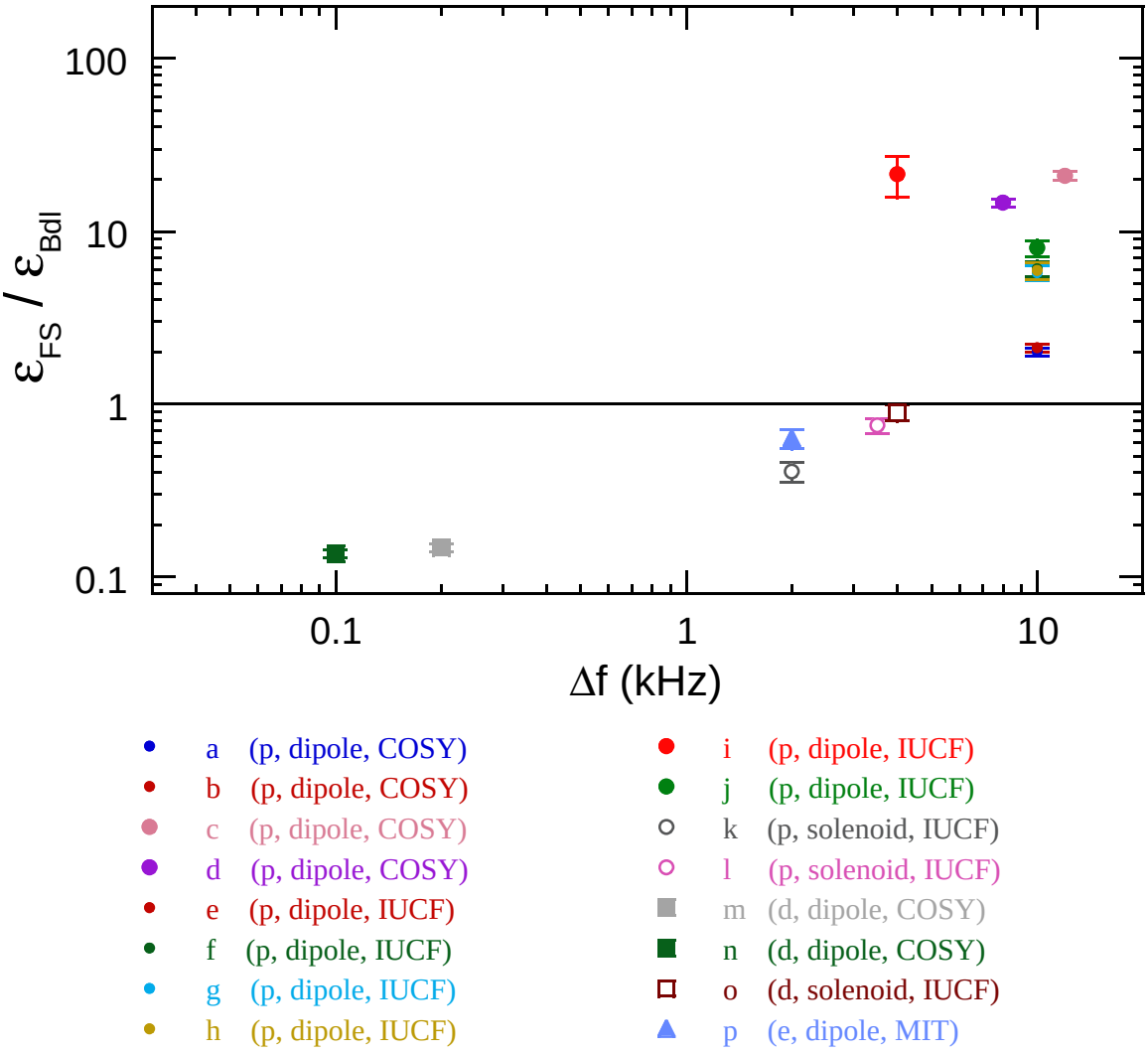

Figure V.1: Ratio of $\mathcal{E}_{FS}$ to $\mathcal{E}_{Bdl}$ is plotted vs. the frequency range Δf used for each Δt curve. The reference and some experimental parameters for each point are listed in Table V.1. For example, points **c** and **d** come from Figs. IV.2 and IV.4, respectively. $\mathcal{E}_{FS}$ is obtained by fitting data in each Δt curve to Eq. (IV.3); $\mathcal{E}_{Bdl}$ is obtained using each data point's $\int Bdl$ in Eq. (V.1) or (V.2). Note that points **a** and **b** overlap, as do points **e**, **f**, **g** and **h**.

dipoles. For protons, all $\mathcal{E}_{FS}/\mathcal{E}_{Bdl}$ ratios were above 1 for rf dipoles, and below 1 for rf solenoids.

Ring, particle and magnet type	Reference	p (GeV/c)	ν_y	Δf (kHz)	Flips	$\mathcal{E}_{Bdl}$ ($\times 10^{-6}$)	$\mathcal{E}_{FS}$ ($\times 10^{-6}$)	$\mathcal{E}_{FS}/\mathcal{E}_{Bdl}$
COSY, p, Dipole	[23]	1.941	3.60	10	11	9.8	19.7±0.3	2±0.1
				10	1		20.7±0.2	2.1±0.1
COSY, p, Dipole	[32]	2.100	3.525	12	11	39.90	840±30	21±1
				8	1		583±9	14.5±0.8
IUCF*, p, Dipole	[22]	0.489	0.15	10	1	33.35	199±2	6.0±0.6
				10	10		202±4	6.0±0.6
IUCF*, p, Dipole	[21]	0.489	0.22	10	10	35.44	204±3	5.8±0.6
				10	1		210±9	6.0±0.6
IUCF, p, Dipole	[18]	0.649	4.791	4	1	7.02	150±40	22±6
IUCF*, p, Dipole	[19]	0.489	0.2	10	1	8.85	71±3	8.0±0.8
IUCF*, p, Solenoid	[27]	0.454		2	1	235	95±8	0.40±0.06
IUCF, p, Solenoid	[25]	0.529		3.5	1	176	133±2	0.76±0.08
COSY, d, Dipole	[30]	1.850	3.60	0.2	1	7.9	1.166±0.009	0.15±0.01
COSY, d, Dipole	[29]	1.850	3.60	0.1	1	2.19	0.298±0.006	0.14±0.01
IUCF, d, Solenoid	[28]	1.042	0.201	4	1	19.44	17.3±0.6	0.88±0.09
MIT*, e, Dipole	[31]	0.670	8.183	2	1	8.9	5.6±0.4	0.64±0.08

Table V.1: Some experimental parameters for the data in Fig. V.1. The letters p, d and e stand for protons, deuterons and electrons, respectively. We assumed a ±10% error in the rf magnets' $\int Bdl$ for the experiments at IUCF and MIT, and a ±5% error in the rf dipole's $\int Bdl$ for our experiments at COSY. The $*$ denotes experiments done with a $\sim 100\%$ Siberian snake present in the ring.

V.1.2 Strength of an RF-Dipole-Induced Resonance

One source of the disagreement between the measured resonance strength and the calculations using Eq. (V.2) for an rf dipole, is that its horizontal magnetic field excites vertical forced beam oscillations [44, 47, 48]. These oscillations occur at the rf dipole's frequency, and their amplitude is proportional to the rf dipole's strength, Eq. (II.38). These oscillations drive the beam into the horizontal fields of ring's quadrupoles; thus, the rf dipole itself is no longer the only source of perturbing horizontal magnetic fields at this frequency of $f_r = f_c(k \pm G\gamma)$. Thus, in tune space the rf-induced spin resonances occur at

$$\nu_r \equiv l \pm \frac{f_r}{f_c} = m \pm G\gamma. \tag{V.3}$$

Now consider the case when this tune is close to the vertical betatron tune ν_y of an intrinsic resonance, whose value is given by Eq. (II.15) to be

$$\nu_s \equiv G\gamma = \nu_y + n, \tag{V.4}$$

where k, l, m and n are integers. The perturbations due to ring's quadrupoles' horizontal magnetic fields then add up coherently for many turns around the ring, significantly increasing the rf-induced resonance strength. The resonance strength ε can then be written [44] as a sum of two terms

$$\varepsilon_{FS} = \varepsilon_{Bdl}(A + \frac{B}{|\nu_y - \nu_r|}), \tag{V.5}$$

where the first term is due to the rf dipole's field itself, and the second term is due to the ring's quadrupoles' fields that particles see because of their forced oscillations due to the rf dipole. The second term is also proportional to the rf dipole's strength ε_{Bdl} because the amplitude of the forced oscillations is proportional to the rf-dipole's strength.

V.2 RF-Dipole-Induced Resonance Strength for Protons

During our November 2005 run, we experimentally studied the resonance strength deviations using the rf dipole, by varying its voltage, and the size, momentum spread, and vertical betatron tune of a 2.1 GeV/c polarized proton beam stored in COSY.

The 2.1 GeV/c polarized proton beam was similar to that described in section IV.2 for the high efficiency spin-flipping experiment. The main difference was that we used the electron Cooler to reduce the beam's size and momentum spread at injection energy. A 24.5 keV electron beam of about 170 mA, with a diameter of about 25 mm,

cooled the protons in COSY's 2-m-long cooling section; it took 10 s to cool the proton beam's momentum spread $\Delta p/p$ and transverse emittance. This decreased its injected momentum spread by about a factor of 2 to about $\Delta p/p = 2.4 \times 10^{-4}$ FWHM. The measured flat-top polarization, before spin manipulation, was typically 50 to 60%.

V.2.1 The Spin Resonance Search

We first determined the resonance's position and the upper limit on its width using the procedure described in section IV.2.1. Fitting the ± 0.2 kHz data to a first-order Lorentzian gave a resonance frequency f_r of 906.5 ± 0.1 kHz and an upper limit on the resonance width w of 1.1 ± 0.2 kHz FWHM. Comparing these to the results in Fig. IV.1, the electron cooling at injection reduced the total measured width of the resonance by about a factor of two, which is consistent with a factor of two reduction in the measured momentum spreads $\Delta p/p$, while the resonance position moved by about 4 kHz, which may be due to the slightly different accelerator parameters used when the electron cooling was on or off. Based on these data and the experiment

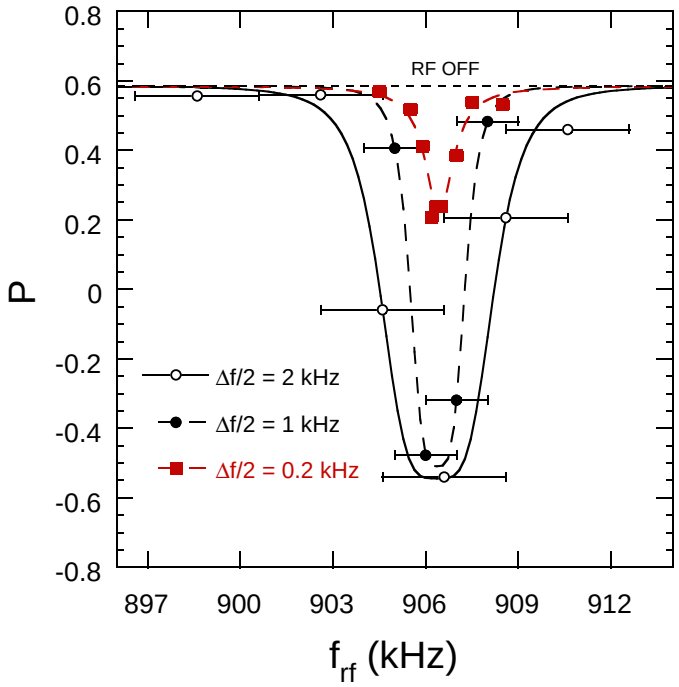

Figure V.2: The measured proton polarization is plotted against the central frequency of each ramp; each ramp's full-frequency range Δf is shown by a horizontal bar; the $\Delta f/2$ values of each ramp are indicated by the different symbols in the figure. The ramp time Δt was set at 2 s. The curves are fits using 1^{st}-order Lorentzian for ± 0.2 kHz sweeps and 2^{nd}-order Lorentzians for ± 1 and ±2 kHz sweeps.

discussed in Chapter IV, we chose $\Delta f/2 = 4$ kHz for further studies.

V.2.2 RF Dipole Voltage Study

We next studied the dependence of the measured resonance strength ε_{FS} on the rf dipole's strength. According to Eq. (V.2) the strength is proportional to the rf dipole's $\int Bdl$, which is proportional to the rf voltage across the dipole. After one spin-flip, we measured the final polarization P_f while varying the rf-dipole's voltage and keeping the other resonance crossing parameters fixed at $\Delta f = 8$ kHz and $\Delta t = 4$ ms. For each P_f measurement, the effective resonance strength was obtained by using Eq. (V.6), the inverted Froissart-Stora equation (Eq. (I.4)).

$$\varepsilon_{FS} = \frac{1}{\pi f_c}\sqrt{\frac{\Delta f}{\Delta t}\ln\frac{2}{P_f/P_i + 1}}. \tag{V.6}$$

For each value of the rf dipole voltage, P_f was the final measured polarization while P_i was taken as the polarization measured at zero voltage. These data are plotted against the rf dipole voltage in Fig. V.3. The data are described very well by a straight line going through zero; thus, the measured resonance strength is indeed proportional to the rf dipole's $\int Bdl$.

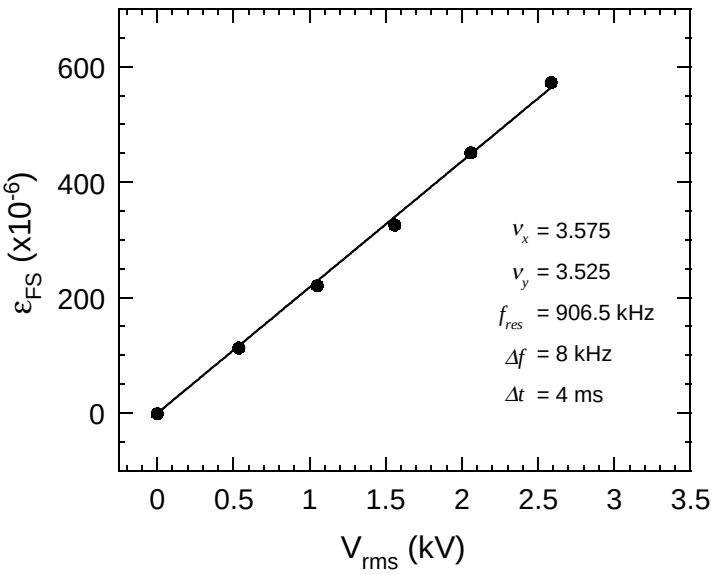

Figure V.3: The rf-induced resonance strength ε_{FS} is plotted against the rf-dipole's voltage; the ramp's full-frequency range Δf was set at 8 kHz and the ramp time Δt was set at 4 ms.

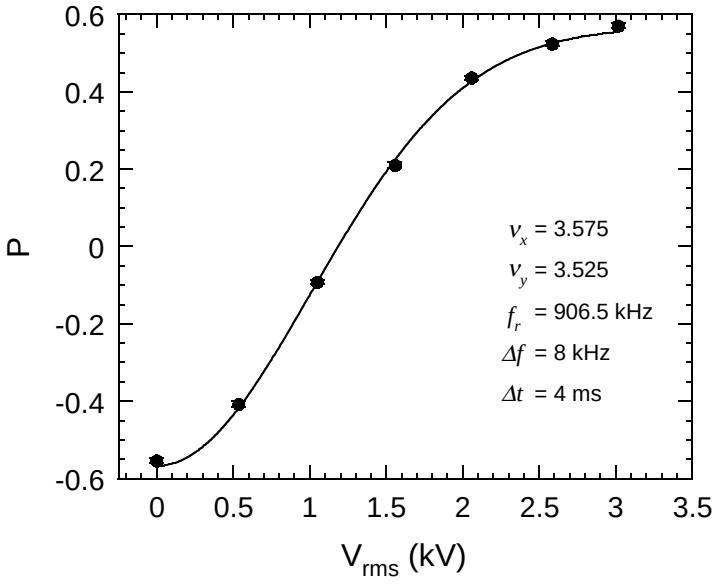

Figure V.4: The measured proton polarization is plotted against the rf-dipole's voltage; the ramp's full-frequency range Δf was set at 8 kHz and the ramp time Δt was set at 4 ms. The curve is fit to Eq. (I.4).

The measured final polarization after one flip is also plotted in Fig. V.4. The fit to the Froissart-Stora equation Eq. (I.4) with $\varepsilon_{FS} = K \times V_{rms}$, where K was a fit parameter, gave a calibration of ε_{FS} against the rf dipole voltage, $K = (212 \pm 2) \times 10^{-6}$ kV^{-1}.

V.2.3 Beam Size Study

COSY uses a fast pulsed quadrupole to produce a vertical betatron tune jump to preserve beam's polarization during acceleration through its intrinsic resonances. The pulse of the fast quadrupole has a 10 μs rise time and 40 ms fall-off time. We pulsed this fast quadrupole at the start of COSY's flat-top to increase the beam's emittance before manipulating the beam's polarization with the rf dipole. We measured beam's vertical profile for several different fast quadrupole currents by moving EDDA's thin fiber target vertically through the beam. We simultaneously recorded the target's position, and measured the current of secondary electrons due to scattering of the beam on the fiber target.

The position of EDDA's target and the secondary electron monitor signal are plotted vs. time in Fig. V.5 for 0 A of current in the fast pulsed quadrupole. We recorded similar data for several other currents in the fast quadrupole. For each data set, we obtained the two time values when the secondary electron monitor signal was at its half maximum value. We then obtained, for those two times, the values of the

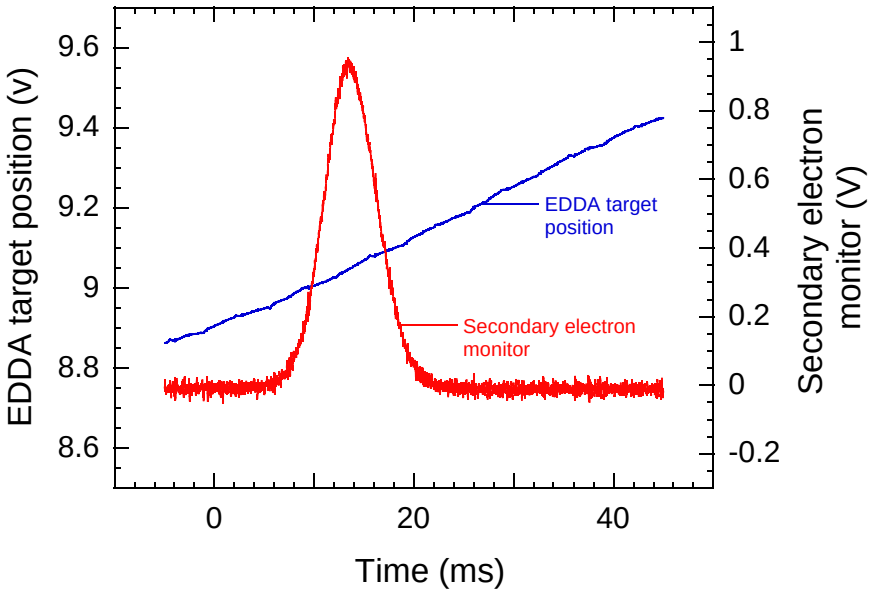

Figure V.5: EDDA target position and Secondary electron monitor signal vs. time for 0 A of current in the fast pulsed quadrupole at the start of COSY's flat-top.

EDDA target position signals in volts. Then we divided their voltage difference by a calibration constant of 0.033 mm/V, to obtain the beam's vertical full width at half maximum Δy_{FWHM} size. This is plotted in Fig. V.6 against the current in the fast quadrupole.

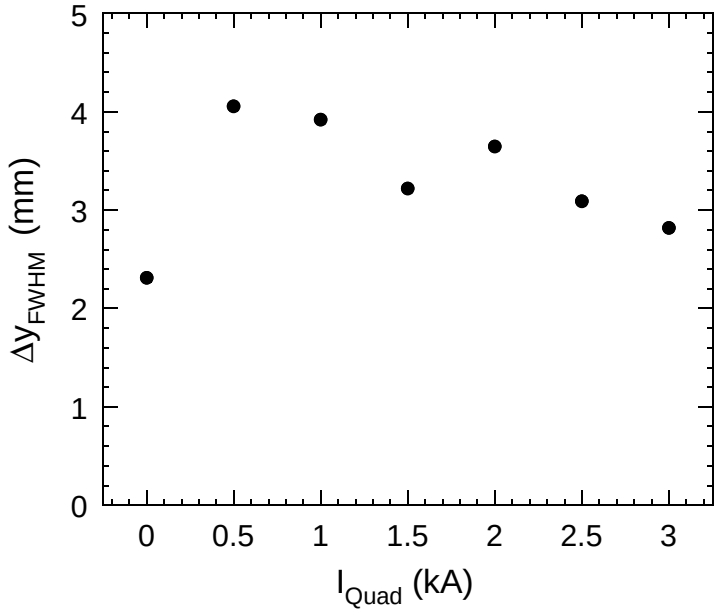

Figure V.6: The beam's measured vertical size Δy_{FWHM} vs. current in the fast quadrupole.

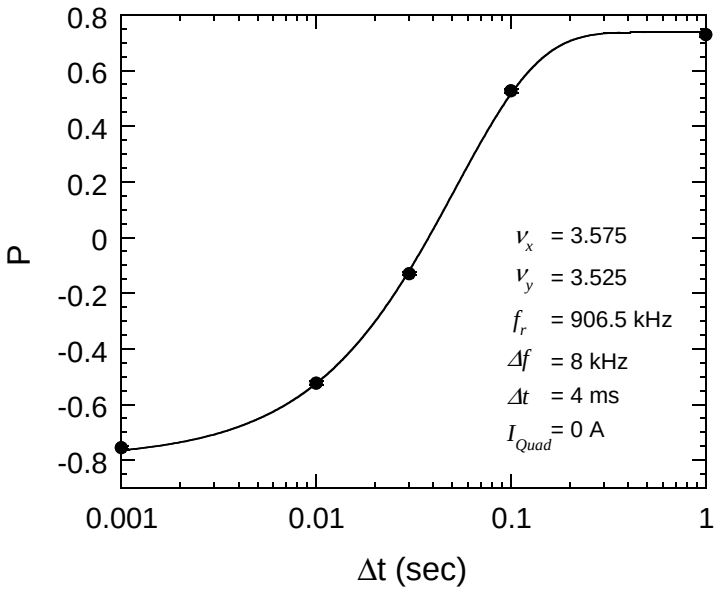

Figure V.7: The proton final polarization measured after 1 spin-flip, is plotted against the rf dipole's ramp time Δt. The curve is a fit to Eq. (I.4), giving the measured resonance strength ε_{FS} of $(84.0 \pm 0.6) \times 10^{-6}$. The resonance strength ε_{Bdl} calculated from Eq. (V.2) was $(6.7 \pm 0.3) \times 10^{-6}$.

While the data are not very precise and it is difficult to estimate the systematic errors, it seems to indicate that the beam size increased by a factor of about 2 for moderate pulsed quadrupole currents, but then stopped increasing probably due to beam losses when the beam size exceeded COSY's acceptance range. Nevertheless, we used the obtained values in Fig. V.6 as the vertical beam size values for those fast quadrupole currents.

Then, we obtained the resonance strength ε_{FS} from Δt curves for few different currents in the fast quadrupole. A typical Δt curve from this study, for 0 A current in the fast quadrupole, is shown in Fig. V.7. We plotted the final beam polarization, measured after one spin-flip for different frequency ramp times Δt and all other parameters fixed, against its Δt; we then obtained the resonance strength ε_{FS} from a fit to Eq. (I.4).

The $\varepsilon_{FS}/\varepsilon_{Bdl}$ ratios for 1, 2 and 3 A currents in the fast quadrupole are plotted in Fig. V.8 against the beam's vertical size Δy_{FWHM} which was obtained for that fast quadrupole current value and is shown in Fig V.6. The slightly-higher ε_{FS} / ε_{Bdl} ratio value at 0 A current is only about 3% higher, which is visible only on the very blown-up scale, while the beam size was increased by more than 30%. Thus, the data show no dependence on the beam's vertical size. The fit to horizontal straight line gives resonance strength ratio of 12.1 $\pm$ 0.1.

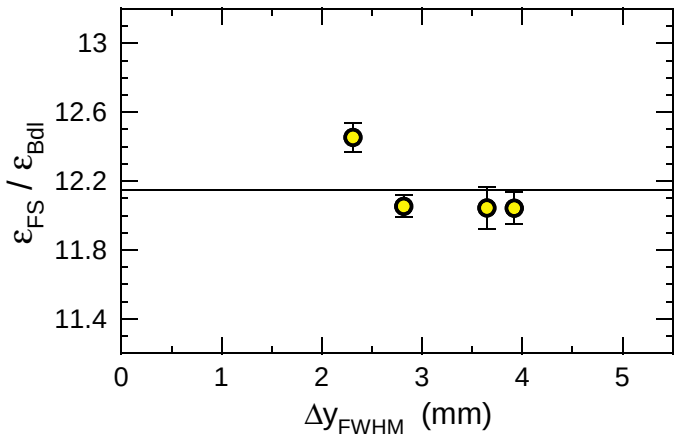

Figure V.8: Ratio of $\mathcal{E}_{FS}$ to $\mathcal{E}_{Bdl}$ is plotted vs. the vertical beam size Δy_{FWHM}. Fit to horizontal straight line gives a resonance strength ratio of 12.1 ± 0.1. The vertical betatron tune ν_y was 3.525.

V.2.4 Beam Momentum Spread Study

The presence of electron cooling at injection was essentially the only difference in beam parameters between the November 2005 proton run and the earlier April 2004 proton run described in Chapter IV. This similarity allowed us to directly compare the ratios of the measured rf-induced resonance strengths to the calculated strength using $\int Bdl$, for these two experiments. For the earlier experiment, the momentum spread $\Delta p/p$ was about 5×10^{-4} FWHM, while for this experiment $\Delta p/p$ was reduced to about 2.4×10^{-4} FWHM.

We earlier measured an $\mathcal{E}_{FS}/\mathcal{E}_{Bdl}$ ratio of 14.5±0.8 for a single spin flip in Fig. IV.2; while we measured an average ratio of 12.1 ± 0.1 for single spin flips for the different beam sizes in Fig. V.8. These two results differ by only about 15%, while both are about 13 times too high; thus, momentum fluctuations can not be responsible for these large deviations of measured rf-induced resonance strength from the strengths calculated using Eq. (V.2).

V.2.5 Vertical Betatron Tune Study

We measured the proton beam's final polarization after sweeping, on flat-top, the vertical betatron tune ν_y from its initial value of 3.525 to different final values, to study the nearby 1^{st}-order intrinsic spin resonance $\nu_s = 8-\nu_y$, which was expected at $\nu_y = 8-4.395 = 3.605$ for the 2.1 GeV/c proton beam. These data are plotted vs. the final value of ν_y in Fig. V.9. During injection into COSY and acceleration, the vertical ν_y and horizontal ν_x betatron tunes were fixed at 3.525 and 3.575, respectively. Next

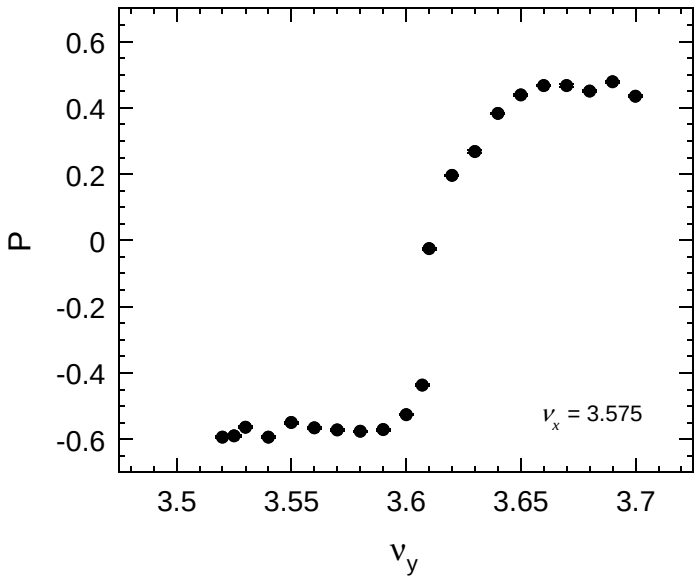

Figure V.9: The final proton polarization, measured after the vertical betatron tune ν_y was moved at the start of COSY's flat-top time from its original value of 3.525 to some final value of ν_y, is plotted vs. the final ν_y. The horizontal betatron tune ν_x was fixed at 3.575; the rf dipole was off.

ν_y was moved, at the start of COSY's flat-top, from 3.525 to some final value, while ν_x was fixed at 3.575; then, the final proton polarization was measured. The rf dipole was off during this study.

Figure V.9 shows that the polarization flipped as we crossed this 1^{st}-order $\nu_s = 8 - \nu_y$ resonance; this suggests that this resonance was rather strong. The 2.1 Gev/c proton beam momentum placed the 1^{st}-order intrinsic resonance in the ν_y region where COSY could operate; thus, we could study the rf resonance strength in proximity of a strong intrinsic resonance. There were also four 3^{rd}-order and one 2^{nd}-order much weaker resonances in the accessible ν_y range.

We then obtained the resonance strength ε_{FS} from Δt curves similar to Fig. V.7 for different values of the vertical betatron tune ν_y. The resulting $\varepsilon_{FS}/\varepsilon_{Bdl}$ ratios are plotted against ν_y in Fig. V.10. The dependence of $\varepsilon_{FS}/\varepsilon_{Bdl}$ on the distance between the vertical betatron tune ν_y and the rf spin resonance's tune ν_r is given by Eq. (V.5). Fitting the data in Fig. V.10 to Eq. (V.5) gave A of 0.87 $\pm$ 0.92, B of 1.01 $\pm$ 0.06; moreover ν_r was 3.6060 $\pm$ 0.0005, which was very near the calculated value of 3.605 for the 1^{st}-order intrinsic spin resonance. The parameter B depends on many details of the ring. The parameter A should give the predicted resonance strength ratio $\varepsilon_{FS}/\varepsilon_{Bdl}$ infinitely far from any intrinsic spin resonances [36, 42, 43, 45, 46]. Clearly our data could not determine A with good precision. The data in Fig. V.10 along with some relevant experimental parameters are listed in Table V.2.

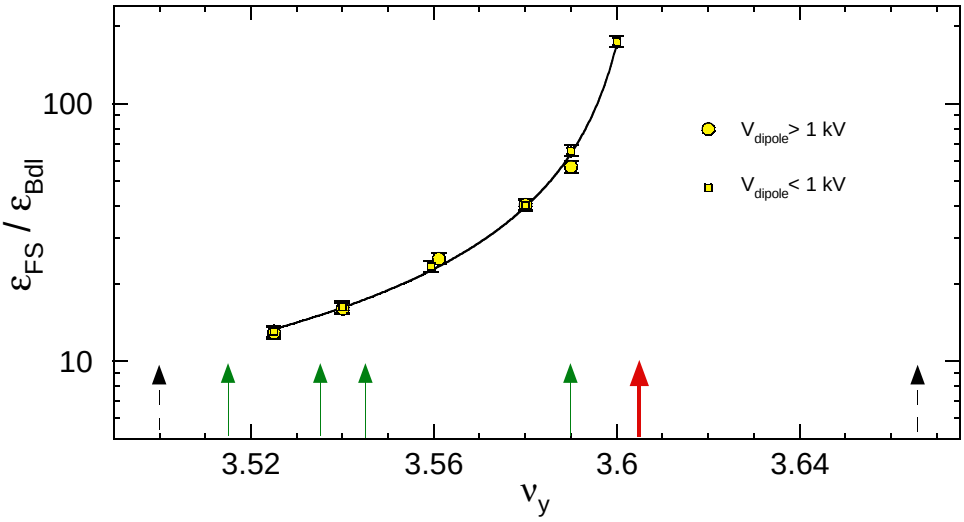

Figure V.10: Ratio of $\mathcal{E}_{FS}$ to $\mathcal{E}_{Bdl}$ is plotted vs. the vertical betatron tune ν_y. The fit to Eq. (V.5), gives ν_r of 3.6060 $\pm$ 0.0005, A of 0.87 $\pm$ 0.92 and B of 1.01 $\pm$ 0.06. The 1^{st} and 3^{rd} order proton spin resonances are shown by the red (bold) and green arrows, respectively. The betatron beam resonances are shown by the black dashed arrows. Some experimental parameters for each data point are listed in Table V.2.

Ring, particle and magnet type	p (GeV/c)	ν_y	Flips	$\mathcal{E}_{Bdl}$ ($\times 10^{-6}$)	$\mathcal{E}_{FS}$ ($\times 10^{-6}$)	$\mathcal{E}_{FS}/\mathcal{E}_{Bdl}$
COSY, p, Dipole	2.100	3.525	1	49.6	634±10	12.8±0.6
		3.525	1	3.9	50.6±0.4	13.0±0.6
		3.540	1	2.18	35.2±0.5	16.2±0.8
		3.540	1	8.5	135±1	15.8±0.8
		3.559	1	2.18	50.3±0.2	23±1
		3.561	1	17.5	434±2	25±1
		3.580	1	17.5	705±3	40±2
		3.580	1	1.13	45.2±0.2	40±2
		3.590	1	17.5	988±9	57±3
		3.590	1	1.13	73.6±0.3	65±3
		3.600	1	1.13	195±1	172±8

Table V.2: Data for Fig. V.10 along with some relevant experimental parameters. We assumed a ±5% normalization uncertainty in the rf dipole's $\int Bdl$, which dominated the $\mathcal{E}_{FS}/\mathcal{E}_{Bdl}$ error in the error.

V.3 RF-Dipole-Induced Resonance Strength for Deuterons

During our December 2004 deuteron run, we varied the beam's vertical size, and the rf dipole's voltage; during our May 2006 deuteron run, we varied the rf dipole's frequency sweep range Δf, and the momentum spread $\Delta p/p$ and betatron tune ν_y of stored 1.85 GeV/c polarized deuterons.

The beam emerging from the polarized D^- ion source was accelerated by the cyclotron to COSY's injection energy of about 75.7 MeV. Then the Low Energy Polarimeter measured the deuteron's polarization before injection into COSY to monitor the stable operation and polarization of the ion source. The Electron Cooler reduced the beam's size and momentum spread at injection energy. A 20.6 keV electron beam cooled the deuteron beam's transverse emittances and momentum spread $\Delta p/p$. The EDDA detector measured the beam's polarization in COSY; we reduced its systematic errors by cycling the polarized source between the 5 different vector and tensor vertical polarization states used in December 2004:

$$(P_V, P_T) = (0,0), (+\tfrac{1}{2}, +\tfrac{1}{2}), (\tfrac{1}{3}, -1), (+\tfrac{2}{3}.0), (0, -2),$$

or the 4 different vector and tensor vertical polarization states used in May 2006:

$$(P_V, P_T) = (0,0), (+1, +1), (\tfrac{1}{3}, -1), (-\tfrac{2}{3}, 0)$$

on sequential pulses. The rf acceleration cavity was turned off and shorted during COSY's flat-top. The measured (+1,+1) vector polarization, before spin manipulation, was about 63%.

In COSY, the deuterons' average circulation frequency f_c was 1.147 43 MHz at 1.850 GeV/c, where their Lorentz energy factor was $\gamma = 1.4046$. For these parameters, the spin tune $\nu_s = G\gamma$ was $-0.200\ 84$. Thus, Eq. (IV.2) implies that the $f_r = f_c(1 + G\gamma)$ spin resonance's central frequency should be very near 917.0 kHz.

We manipulated the deuteron's polarization using the ferrite-core rf dipole, with an 8-turn copper coil, which produced a uniform radial magnetic field. The rf dipole was part of an LC resonant circuit, which operated near $f_r = 917$ kHz, typically at an rf voltage of 3.1 kV rms giving an rf $\int B_{rms} dl$ of 0.60 ± 0.03 T·mm. Thus, Eq. (V.2) gives an ε_{Bdl} of $(8.8 \pm 0.4) \times 10^{-6}$.

V.3.1 RF Dipole Voltage and Beam Size Studies with Deuterons

The main focus of the December 2004 run, was on coherent partial spin rotations rather than on studying the rf-dipole-induced resonance strength for deuterons. We did only a few studies relevant to the rf resonance strength investigation.

After determining the position and width of the rf resonance, we studied the dependence of the measured resonance strength ε_{FS} on the rf dipole's voltage. We

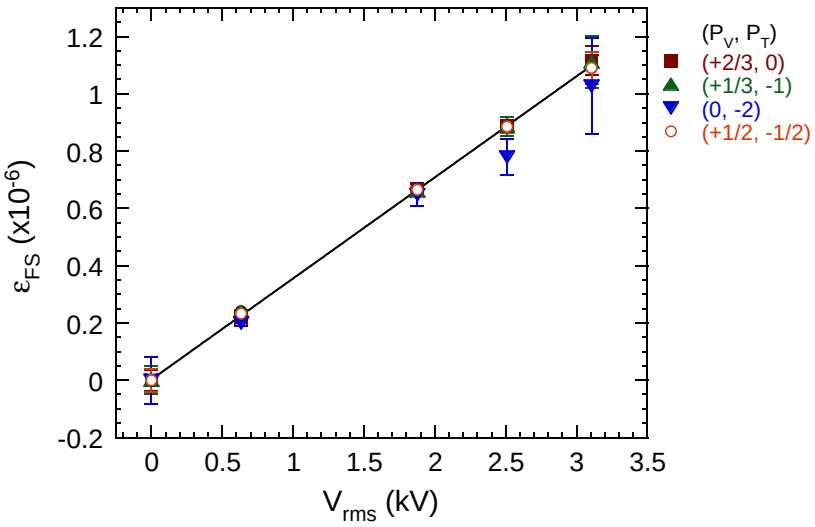

Figure V.11: The measured rf-induced resonance strength $\mathcal{E}_{FS}$ is plotted against the rf-dipole's voltage for each of the 4 non-zero deuteron polarization states; the ramp's frequency range Δf was set at 150 Hz and the ramp time Δt was set at 30 s.

measured the final deuteron vector polarization for each polarization state after a single frequency sweep, while varying the rf-dipole's voltage with the resonance crossing parameters Δf and Δt fixed at $\Delta f = 150$ Hz and $\Delta t = 30$ s. For each value of the rf dipole voltage, we obtained the effective resonance strength $\mathcal{E}_{FS}$ from the measured deuteron vector polarization using Eq. (V.6). These data are plotted against the rf dipole voltage in Fig. V.11. It shows that the deuteron's measured rf resonance strength seems to be proportional to the rf dipole's $\int Bdl$.

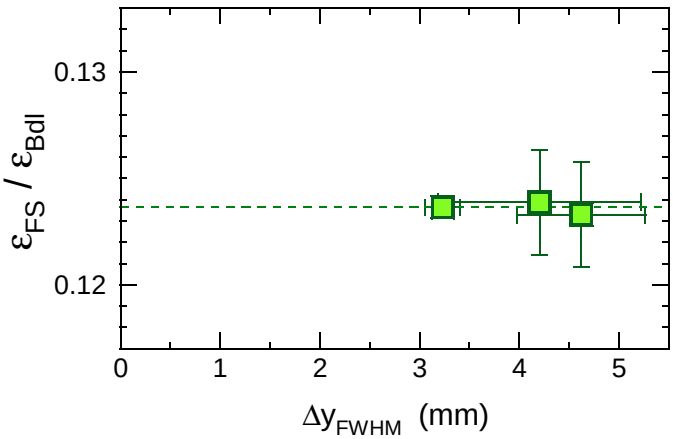

Figure V.12: Ratio of $\mathcal{E}_{FS}$ to $\mathcal{E}_{Bdl}$ is plotted vs. the vertical beam size Δy_{FWHM}. The vertical betatron tune ν_y was 3.60. The fit to a horizontal line gives a resonance strength ratio of 0.12 ± 0.01.

We then studied the dependence of the measured resonance strength $\mathcal{E}_{FS}$ on the vertical beam size as described in Section V.2.3. We used the fast quadrupole to increase the beam's vertical size. For each beam size, we obtained $\mathcal{E}_{FS}$ by taking a Δt-curve at the rf dipole's maximum voltage with $\Delta f = 200$ Hz. The $\mathcal{E}_{FS}/\mathcal{E}_{Bdl}$ ratios are plotted against the beam's vertical size Δy_{FWHM} in Fig. V.12. The data are consistent with no dependence on the beam's vertical size; the data's fit to a horizontal line gives a $\mathcal{E}_{FS}/\mathcal{E}_{Bdl}$ ratio of 0.12 ± 0.01.

V.3.2 Deuteron Spin Resonance Search

Our May 2006 run with deuterons was mostly focused on studying the rf-dipole-induced resonance strength. We also studied and tried to confirm a new matrix formalism developed by A.W. Chao [75, 76] that describes a crossing of an isolated spin resonance in a more general way than Froissart and Stora's 1960 paper [17].

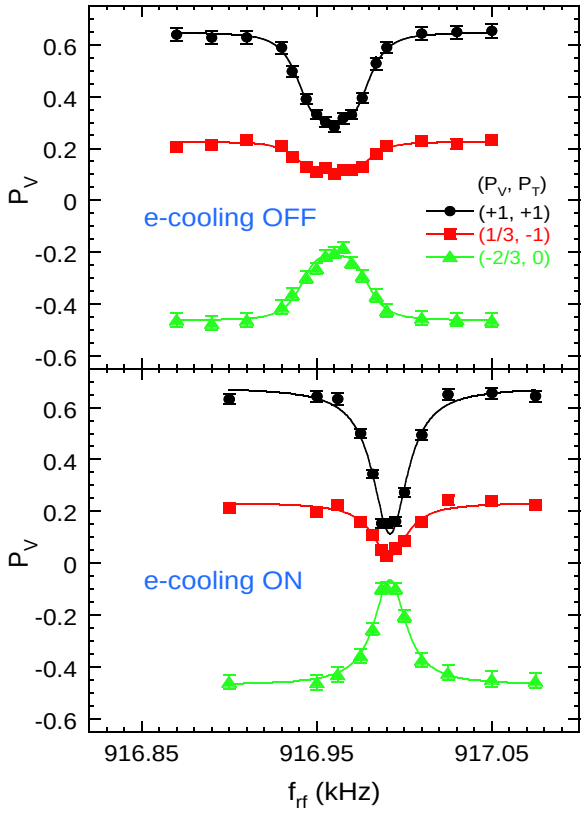

Figure V.13: Measured vector deuteron polarizations at 1.85 GeV/c are plotted vs rf-dipole frequency f_{rf}. Fits of the e-cooling OFF data to a 2^{nd}-order Lorentzian give a resonance frequency f_r of $916,960 \pm 10$ Hz and width w of 42 ± 2 Hz FWHM. Fits of the e-cooling ON data to a 1^{st}-order Lorentzian give f_r of $916,992 \pm 10$ Hz and w of 23 ± 2 Hz FWHM.

We first determined the rf resonance's position, with the electron cooling both on and off, by measuring the polarization with the rf dipole set at different fixed frequencies. These data are shown in Fig. V.13. Note that the deuteron rf-resonance frequency changed by about 30 Hz, probably due to slightly different COSY parameters that somehow occurred when the electron cooling was on or off. The electron cooling decreased the resonance's total width w from 42 ± 2 to 23 ± 2 Hz FWHM. The resonance's natural width, $2\varepsilon_{FS} f_c$, was only 3 Hz; thus, the total width was dominated by the resonance width due to the beam's momentum spread $\Delta p/p$. When the natural width is unfolded from the measured w values, the resulting resonance width values due to the beam's $\Delta p/p$ (42 ± 2 and 23 ± 2) are essentially the same as the measured total width values.

V.3.3 RF-Dipole Frequency Ramp Range Δf and Beam Momentum Spread Studies with Deuterons

All earlier anomalous deuteron $\varepsilon_{FS}/\varepsilon_{Bdl}$ data [33] were at the small Δf values of 100 and 200 Hz; thus, we increased Δf in four steps from 100 to 3000 Hz. The resulting $\varepsilon_{FS}/\varepsilon_{Bdl}$ ratios, at $\nu_y = 3.60$, are plotted vs Δf in Fig. V.14 along with all earlier deuteron data. The data show no dependence of $\varepsilon_{FS}/\varepsilon_{Bdl}$ on Δf.

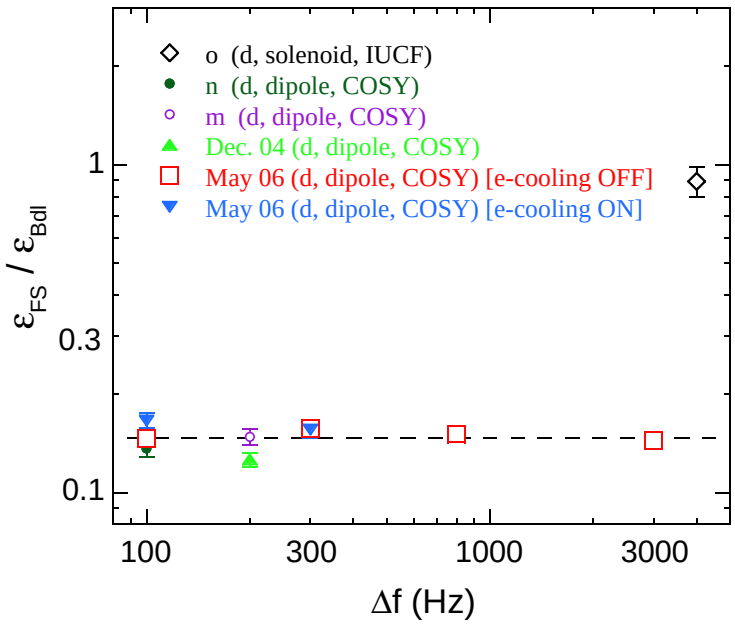

Figure V.14: Ratio of ε_{FS} to ε_{Bdl} for deuterons is plotted vs rf dipole's frequency sweep range Δf. The ν_y values at COSY were all 3.60, and ν_y was 4.80 at IUCF. ε_{FS} is the resonance strength obtained by fitting the Δt curve for each data point to Eq. (IV.3); ε_{Bdl} was obtained using each data point's $\int Bdl$ in Eq. (V.1) or (V.2). The fit to all rf dipole deuteron points gives a resonance strength ratio of 0.15 ± 0.01.

We also measured ε_{FS} for two different frequency ranges, Δf of 100 and 300 Hz, with the beam's momentum spread reduced by the electron cooler. These data are also shown in Fig. V.14. The $\varepsilon_{FS}/\varepsilon_{Bdl}$ ratios for the cooled and uncooled beams differ only by about 7%, while Fig. V.13 indicates that the cooling reduced $\Delta p/p$ by a factor of 2. Thus, any small $\Delta p/p$ fluctuations can not explain the observed 7-fold reduction of the resonance strength for experiments with both cooled and uncooled beams. The fit to all rf-dipole points gives a resonance strength $\varepsilon_{FS}/\varepsilon_{Bdl}$ ratio of 0.15 ± 0.01 for deuterons, which certainly disagrees with Eq. (V.2). However we noted that the IUCF rf-solenoid point [28] had $\varepsilon_{FS}/\varepsilon_{Bdl}$ quite near to 1.

V.3.4 Vertical Betatron Tune Study with Deuterons

We next measured ε_{FS} for different values of the vertical betatron tune ν_y. The $\varepsilon_{FS}/\varepsilon_{Bdl}$ ratios are plotted against ν_y in Fig. V.15a. The nearby deuteron 1^{st}-order intrinsic spin resonance $\nu_s = \nu_y - 4$ (see Fig. V.15b), allowed a study of the interference between an rf-dipole-induced spin resonance and an intrinsic spin resonance. We fit the observed asymmetric dependence of $\varepsilon_{FS}/\varepsilon_{Bdl}$ on the distance between ν_y and the rf spin resonance's tune $\nu_r \equiv k \pm f_r/f_c$ (where k is an integer) by empirically modifying the earlier-derived hyperbola [33, 44] into an asymmetric hyperbola

$$\varepsilon_{FS}/\varepsilon_{Bdl} = |A + \frac{B}{\nu_r - \nu_y}|. \tag{V.7}$$

Fitting the deuteron data in Fig. V.15a to Eq. (V.7) gave: A of 0.06 ± 0.04, B of 0.010 ± 0.002 and ν_r of 3.798 ± 0.001. This ν_r value was consistent with the expected value of 3.79923 ± 0.00001, calculated from

$$\nu_r = 3 + f_r/f_c \tag{V.8}$$

using COSY's measured f_c of 1,147,306 Hz and the f_r of $916,960 \pm 10$ Hz measured in Fig. V.13. The B parameter depends on many details of the ring. The parameter A should give the predicted [36, 42, 43, 44, 45, 46] $\varepsilon_{FS}/\varepsilon_{Bdl}$ ratio far from any intrinsic spin resonances.

Figure V.15b shows the measured ratio of the final to initial vector polarizations plotted against the different ν_y values with the rf dipole off. Fitting a 2nd-order Lorentzian to this sharp and narrow dip due to the $\nu_s = \nu_y - 4$ intrinsic resonance, gave a width of $(10 \pm 3) \times 10^{-3}$ FWHM and ν_r of 3.795 ± 0.002, which agrees with the 3.798 ± 0.001 value from Fig. V.15a. Figures V.15a and V.15b may be the first detailed study of a deuteron intrinsic spin resonance.

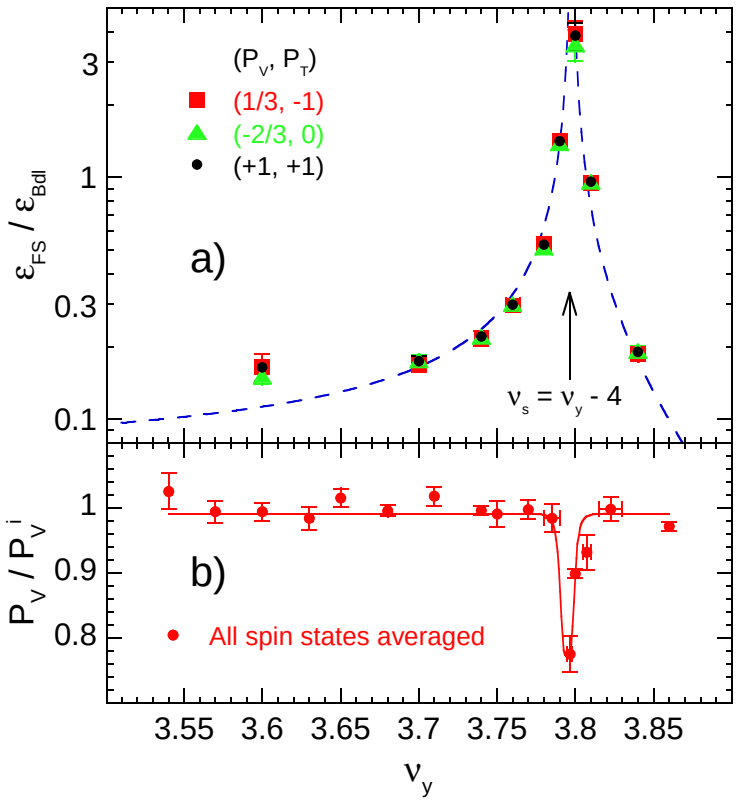

Figure V.15: a) Ratio of $\mathcal{E}_{FS}$ to $\mathcal{E}_{Bdl}$ is plotted vs the vertical betatron tune ν_y; Δf was 300 Hz; the cooling was off. The dashed blue curve is a fit to Eq. (V.7) giving $\nu_r = 3.798 \pm 0.001$. b) Measured deuteron vector polarization ratio at 1.85 GeV/c is plotted vs ν_y; the rf dipole was off; the cooling was on. The red curve is a fit to a 2nd-order Lorentzian giving $\nu_r = 3.795 \pm 0.002$.

V.4 RF-Solenoid-Induced Resonance Strength for Deuterons

During our May 2007 run, we studied the dependence of an rf-solenoid-induced spin resonance's strength $\mathcal{E}_{FS}$ on the rf solenoid's frequency ramp range Δf, and on the momentum spread $\Delta p/p$ and betatron tune ν_y of stored 1.85 GeV/c polarized deuterons. The 1.85 GeV/c vertically polarized deuteron beam was again set up as described in Section V.3 for the experiment with the rf dipole. The only difference was that we used an rf solenoid to manipulate the deuterons' polarization [77]. We cycled the polarized D^- ion source through five different vector P_V and tensor P_T vertical polarization states:

$$(P_V, P_T) = (0, 0),\ (+1, +1),\ (-\tfrac{1}{3}, -1),\ (-\tfrac{2}{3}, 0),\ (-1, +1).$$

The asymmetry measured in the (0, 0) spin state was then subtracted from the other states' measured asymmetries, in each 20 ms time-bin, to correct for detector efficiencies and beam motion asymmetries in the EDDA polarimeter.

The solenoid was a 25-turn air-core water-cooled copper coil, of length 57.5 cm and average diameter 21 cm. It was part of an RLC resonant circuit, which operated near 917 kHz, typically at an rf voltage of 5.7 kV rms producing a longitudinal rf $\int B_{rms} dl$ of 0.67 ± 0.03 T·mm. Thus, Eq. (V.1) gave ε_{Bdl} of $(1.04 \pm 0.05) \times 10^{-5}$.

V.4.1 Deuteron Spin Resonance Search

With e-cooling both off and on for 15 s, we experimentally determined the resonance's center f_r and its width w by measuring the vertical vector polarization P_V after the rf solenoid was run at many different fixed frequencies. These data are plotted vs the rf frequency f_{rf} in Fig. V.16, along with their fit values of f_r and w for the electron cooling off and for the 15 s cooling-time. With 15 s cooling, f_r was 917 010 ± 10 Hz, with electron cooling off, f_r was 916 988 ± 10 Hz; the shift in f_r of about 20 Hz was probably due to slightly different COSY conditions during the electron cooling on and cooling off runs. The fit widths were 86 ± 2 and 41 ± 1 Hz FWHM for the uncooled and cooled beams, respectively, indicating that the momentum spread $\Delta p/p$ was reduced by more than a factor of two.

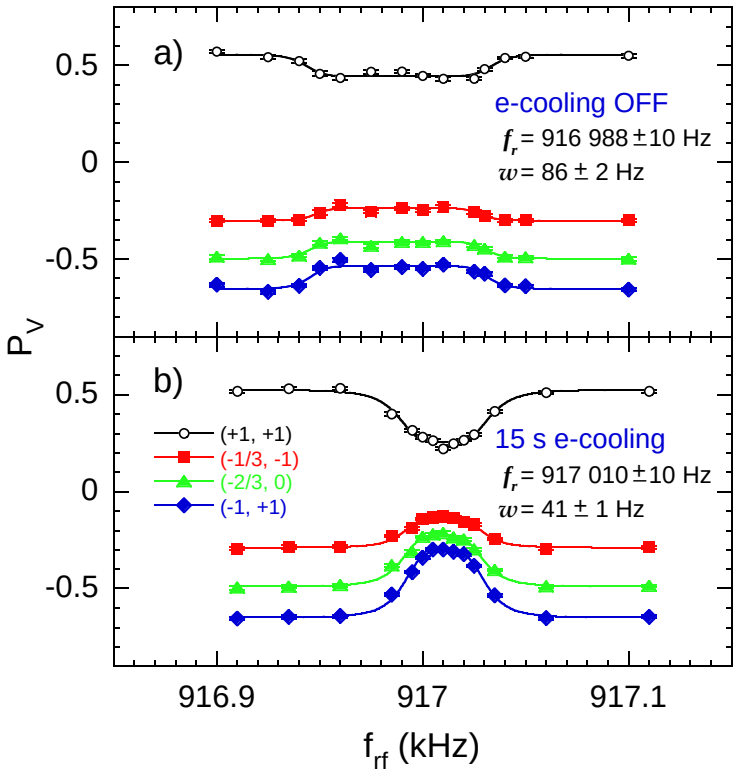

Figure V.16: The measured vertical deuteron vector polarizations at 1850 MeV/c plotted vs the rf-solenoid fixed frequency f_{rf}. The curves are fits to 2nd-order Lorentzians. The data points' errors are purely statistical.

V.4.2 RF Solenoid Frequency Ramp Range Δf and Beam Momentum Spread Studies with Deuterons

All rf dipole data with deuterons showed a resonance strength reduction by about factor of 7; however, the only rf solenoid point [28], which was from IUCF, was quite near to 1. Its frequency ramp range Δf value was 4 kHz, which is significantly larger than the Δf values of 100-200 Hz used with rf dipoles. Thus, we varied the Δf of the new COSY solenoid, in four steps, from 200 to 3000 Hz, with $\nu_y = 3.60$. The resulting $\varepsilon_{FS}/\varepsilon_{Bdl}$ ratios, with an rf solenoid, are plotted vs Δf in Fig. V.17, which shows no dependence of $\varepsilon_{FS}/\varepsilon_{Bdl}$ on Δf.

For two different frequency ranges, Δf of 200 and 300 Hz, we also obtained ε_{FS} with the beam's momentum spread $\Delta p/p$ reduced by the electron cooler. Fig. V.17 shows the $\varepsilon_{FS}/\varepsilon_{Bdl}$ ratios at Δf of 200 and 300 Hz, for both the cooled and uncooled beam; it clearly indicates that the rf resonance strength does not depend on $\Delta p/p$, and it does not depend on Δf.

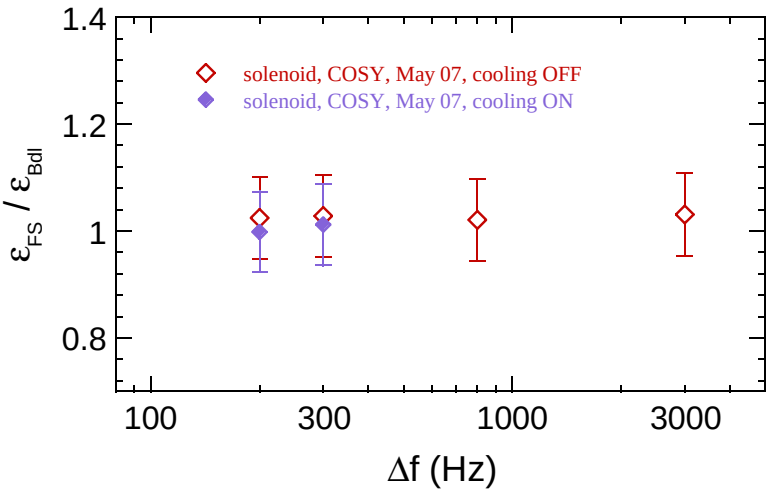

Figure V.17: Ratio of ε_{FS} to ε_{Bdl} for deuterons is plotted vs rf solenoid's frequency sweep range Δf. The ν_y values at were all 3.60. ε_{FS} is the resonance strength obtained by fitting the Δt curve for each data point to Eq. (IV.3); ε_{Bdl} was obtained using each data point's $\int Bdl$ in Eq. (V.1). The errors are strongly dominated by the 5% scale uncertainty in $\int Bdl$.

V.4.3 Vertical Betatron Tune Study with Deuterons

We next measured ε_{FS} for different values of the vertical betatron tune ν_y. The $\varepsilon_{FS}/\varepsilon_{Bdl}$ ratios are plotted against ν_y in Fig. V.18. The data is completely flat, except at ν_y of 3.7975, exactly at the position of the $\nu_s = \nu_y - 4$ deuteron 1^{st}-order intrinsic

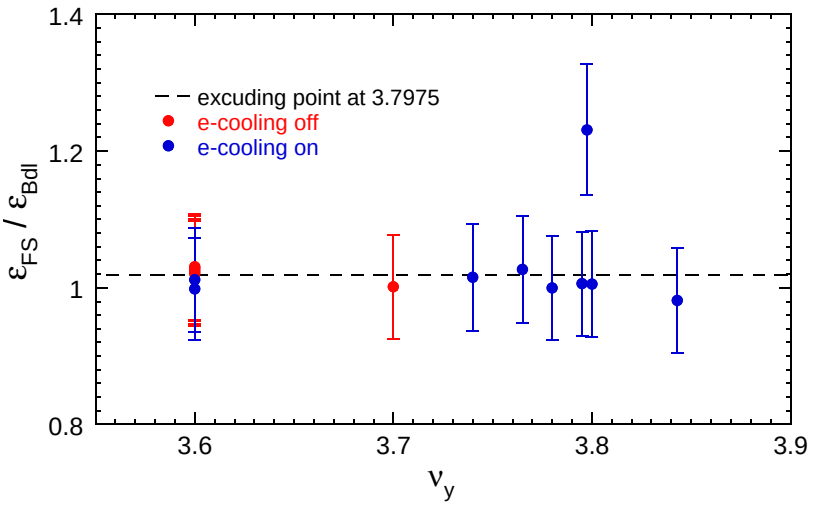

Figure V.18: Ratio of $\mathcal{E}_{FS}$ to $\mathcal{E}_{Bdl}$ is plotted vs the vertical betatron tune ν_y; Δf was 300 Hz. A fit to a horizontal line, excluding the point at $\nu_y = 3.7975$, gives the strength ratio of 1.02 ± 0.05. The errors are again dominated by the 5% scale error in $\int Bdl$.

spin resonance. A fit to a horizontal line, excluding the intrinsic resonance point at $\nu_y = 3.7975$, gives a strength ratio of 1.02 ± 0.05; the error is dominated by the 5% uncertainty in the rf solenoid's $\int Bdl$. These data together with Fig. V.15 confirm that there is no interference with intrinsic spin resonances, since an rf solenoid does not effect the orbital motion of the beam as an rf dipole does. Thus, the formula for the rf spin resonance strength, Eq. (V.1), does not need to be corrected to include the magnetic structure of each accelerator ring.

V.5 Compilation of all RF-Induced Spin Resonance Strength Data

The plot in Fig. V.19 contains all known resonance strength $\mathcal{E}_{FS}/\mathcal{E}_{Bdl}$ ratio data, for protons, deuterons and electrons, including our new experimental data. The proton experiment at COSY [33] showed that the enhancements of the measured rf-induced resonance strengths for protons with rf dipoles, were due to the interference of the rf-induced resonance with a nearby intrinsic resonance. The recent deuteron dipole and solenoid experiments at COSY [34, 78] showed that the 7-fold reductions for deuterons were not due to the small Δf ramps earlier used to manipulate the deuteron spin, or interference with a deuteron intrinsic resonance. There has been some theoretical disagreement about a factor of 2 [42, 43, 44, 45, 46] in both Eqs. (V.1) and (V.2); our deuteron experiment with the rf solenoid at COSY confirms the formula for the rf spin resonance strength with the "BNL" [43, 45] factor of 2.

Recently there has been a theoretical effort to understand what is causing this large reduction in $\mathcal{E}_{FS}/\mathcal{E}_{Bdl}$ for deuterons. An independent approach [79] now challenges

the derivation of Eq. V.2 [36, 41, 42, 43, 44, 45]; it indicates that the factor $(1+G\gamma)$ should instead be $G\gamma$ for the idealistic case where an rf dipole is the only perturbation of spin motion in a circular accelerator or storage ring with no focusing and no radial or longitudinal magnetic fields. It seems that in any real accelerator $\mathcal{E}$ is not exactly proportional to either $G\gamma$ or $(1+G\gamma)$ for an rf dipole. Note that this problem was not noticed earlier because the ratio of $G\gamma$ to $(1+G\gamma)$ is very near one for high energy protons, where it was studied earlier; however, the ratio's magnitude is $|-0.201/0.799| \approx 0.25$ for our 1.85 GeV/c deuterons [34]. Our measured $\mathcal{E}_{FS}/\mathcal{E}_{Bdl}$ ratio of 0.15 ± 0.01 clearly favors the factor $G\gamma$ rather than $(1+G\gamma)$ in Eq. V.2.

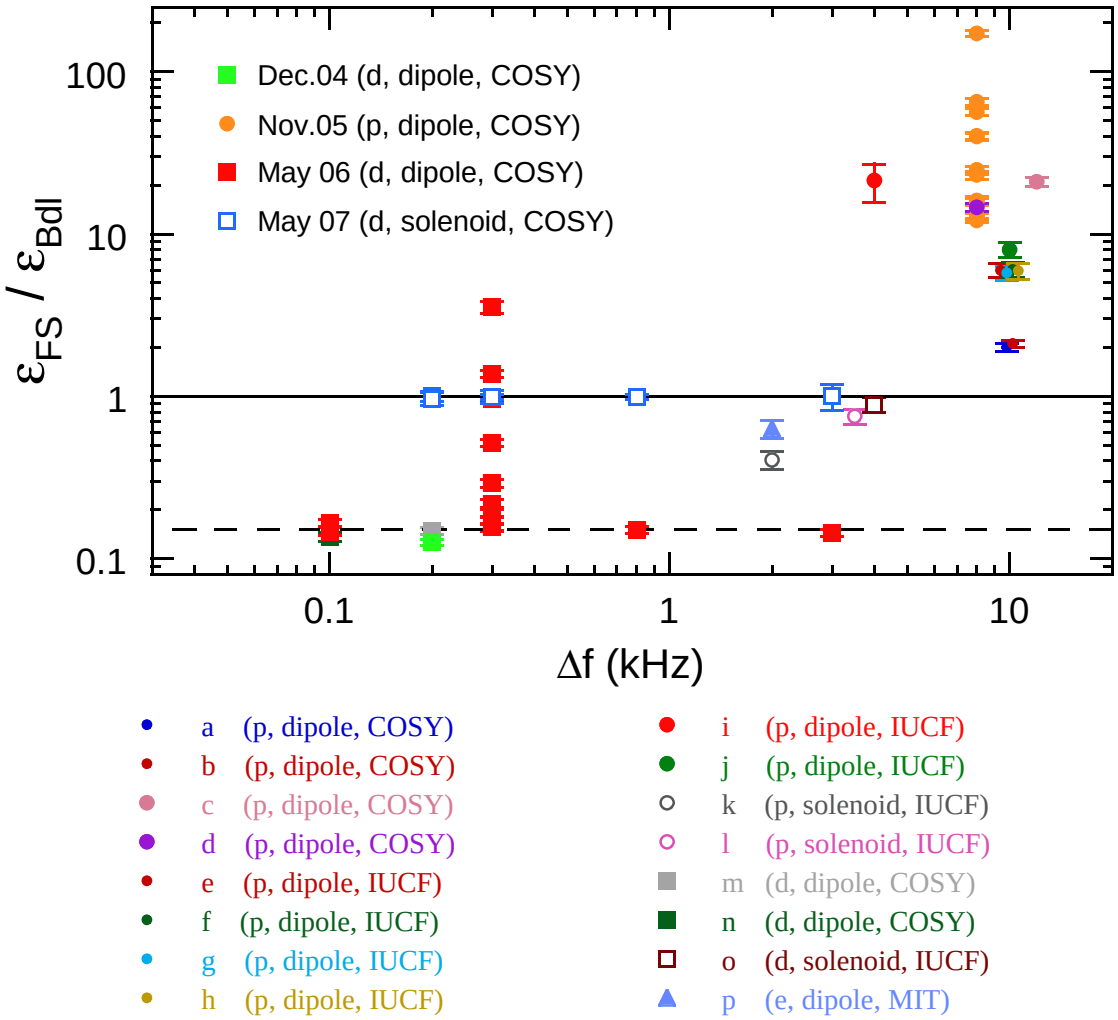

Figure V.19: Ratio of $\mathcal{E}_{FS}$ to $\mathcal{E}_{Bdl}$ is plotted vs. the frequency ramp range Δf used for each Δt curve for all the available data including the new experimental data. $\mathcal{E}_{FS}$ is obtained by fitting data in each Δt curve to Eq. (IV.3) or (I.4); $\mathcal{E}_{Bdl}$ is obtained using each data point's $\int Bdl$ in Eq. (V.1) or (V.2). The solid line is the predicted ratio of 1 for an rf solenoid; the dashed line is the fit to the deuteron rf dipole data. The references and some experimental parameters for each point are listed in Tables V.3 and V.4.

Ring, particle and magnet type	Reference	p (GeV/c)	ν_y	Δf (kHz)	Flips	$\mathcal{E}_{Bdl}$ ($\times 10^{-6}$)	$\mathcal{E}_{FS}$ ($\times 10^{-6}$)	$\mathcal{E}_{FS}/\mathcal{E}_{Bdl}$
COSY, p, Dipole	[23]	1.941	3.60	10	11	9.8	19.7±0.3	2±0.1
				10	1		20.7±0.2	2.1±0.1
COSY, p, Dipole	[32]	2.100	3.525	12	11	39.90	840±30	21±1
				8	1		583±9	14.5±0.8
IUCF*, p, Dipole	[22]	0.489	0.15	10	1	33.35	199±2	6.0±0.6
				10	10		202±4	6.0±0.6
IUCF*, p, Dipole	[21]	0.489	0.22	10	10	35.44	204±3	5.8±0.6
				10	1		210±9	6.0±0.6
IUCF, p, Dipole	[18]	0.649	4.791	4	1	7.02	150±40	22±6
IUCF*, p, Dipole	[19]	0.489	0.2	10	1	8.85	71±3	8.0±0.8
IUCF*, p, Solenoid	[27]	0.454		2	1	235	95±8	0.40±0.06
IUCF, p, Solenoid	[25]	0.529		3.5	1	176	133±2	0.76±0.08
COSY, d, Dipole	[30]	1.850	3.60	0.2	1	7.9	1.166±0.009	0.15±0.01
COSY, d, Dipole	[29]	1.850	3.60	0.1	1	2.19	0.298±0.006	0.14±0.01
IUCF, d, Solenoid	[28]	1.042	0.201	4	1	19.44	17.3±0.6	0.88±0.09
MIT*, e, Dipole	[31]	0.670	8.183	2	1	8.9	5.6±0.4	0.64±0.08
November 2005 experiment								
COSY, p, Dipole	[33]	2.100	3.525	8	1	6.74	84.0±0.6	12.45±0.08
			3.525	8	1	6.74	81.2±0.6	12.04±0.09
			3.525	8	1	6.74	81.2±0.8	12.04±0.12
			3.525	8	1	6.74	81.2±0.4	12.05±0.06
			3.525	8	1	49.6	634±10	12.8±0.6
			3.525	8	1	3.9	50.6±0.4	13.0±0.6
			3.540	8	1	2.18	35.2±0.5	16.2±0.8
			3.540	8	1	8.5	135±1	15.8±0.8
			3.559	8	1	2.18	50.3±0.2	23±1
			3.561	8	1	17.5	434±2	25±1
			3.580	8	1	17.5	705±3	40±2
			3.580	8	1	1.13	45.2±0.2	40±2
			3.590	8	1	17.5	988±9	57±3
			3.590	8	1	1.13	73.6±0.3	65±3
			3.600	8	1	1.13	195±1	172±8

Table V.3: Some experimental parameters for the data in Fig. V.19. The letters p, d and e stand for protons, deuterons and electrons, respectively. We assumed a ±10% error in the rf magnets' $\int Bdl$ for the experiments at IUCF and MIT, and a ±5% error in the rf dipole's or rf solenoid's $\int Bdl$ for our experiments at COSY, which dominated the error in $\mathcal{E}_{FS}/\mathcal{E}_{Bdl}$. The $*$ denotes experiments done with a $\sim 100\%$ Siberian snake present in the ring.

Ring, particle and magnet type	p (GeV/c)	ν_y	Δf (kHz)	Cooling	$\mathcal{E}_{Bdl}$ ($\times 10^{-6}$)	$\mathcal{E}_{FS}$ ($\times 10^{-6}$)	$\mathcal{E}_{FS}/\mathcal{E}_{Bdl}$
December 2004 experiment [33]							
COSY, d, Dipole	1.850	3.60	0.2	off	8.8	1.082±0.003	0.124±0.006
		3.60	0.2	off	8.8	1.16±0.03	0.124±0.007
		3.60	0.2	off	8.8	1.09±0.03	0.123±0.007
May 2006 experiment [34]							
COSY, d, Dipole	1.850	3.60	0.1	off	8.8	1.32±0.03	0.150±0.008
		3.60	0.3	off	8.8	1.39±0.04	0.158±0.008
		3.60	0.8	off	8.8	1.31±0.02	0.149±0.008
		3.60	3	off	8.8	1.25±0.07	0.142±0.008
		3.60	0.1	on	8.8	1.47±0.03	0.167±0.008
		3.60	0.3	on	8.8	1.43±0.05	0.163±0.008
		3.70	0.3	off	8.8	1.53±0.02	0.174±0.008
		3.74	0.3	off	8.8	1.93±0.03	0.219±0.008
		3.78	0.3	off	8.8	4.57±0.07	0.519±0.008
		3.84	0.3	off	8.8	1.68±0.02	0.191±0.008
		3.76	0.3	off	8.8	2.62±0.02	0.298±0.008
		3.80	0.3	off	8.8	33±2	3.77±0.27
		3.79	0.3	off	8.8	12.3±0.1	1.40±0.02
		3.81	0.3	off	8.8	8.43±0.08	0.96±0.01
May 2007 experiment [78]							
COSY, d, Solenoid	1.850	3.60	0.2	off	10.4	10.65±0.06	1.02±0.05
		3.60	0.3	off	10.4	10.69±0.06	1.03±0.05
		3.60	0.8	off	10.4	10.61±0.06	1.02±0.05
		3.60	3	off	10.4	10.72±0.08	1.03±0.05
		3.70	0.3	off	10.4	10.42±0.12	1.00±0.05
		3.74	0.3	on	10.4	10.56±0.20	1.02±0.05
		3.60	0.2	on	10.4	10.38±0.10	1.00±0.05
		3.60	0.3	on	10.4	10.52±0.11	1.01±0.05
		3.78	0.3	on	10.4	10.40±0.15	1.00±0.05
		3.843	0.3	on	10.4	10.21±0.23	0.98±0.05
		3.765	0.3	on	10.4	10.68±0.15	1.02±0.05
		3.80	0.3	on	10.4	10.45±0.21	1.01±0.05
		3.795	0.3	on	10.4	10.46±0.15	1.01±0.05
		3.7975	0.3	on	10.4	12.80±0.28	1.23±0.07

Table V.4: Some experimental parameters for the data in Fig. V.19. The letter d stands for deuterons. We assumed a ±5% error in the rf dipole's or rf solenoid's $\int Bdl$ for our experiments at COSY, which dominated the error in $\mathcal{E}_{FS}/\mathcal{E}_{Bdl}$.

CHAPTER VI

CONCLUSIONS

The ability to control and manipulate a proton or deuteron beam's polarization can greatly reduce the systematic errors in many polarized scattering experiments. We studied the spin-flipping and spin-manipulation of polarized proton and deuteron beams of about 2 GeV at COSY, where we obtained some interesting and unexpected deuteron data and demonstrated very highly efficient proton spin flipping.

We first designed at Michigan a ferrite-core water-cooled rf-dipole, which was then built at COSY using Michigan ferrite. We ramped its frequency through an rf-induced spin resonance to spin-flip the polarization of 2.1 GeV/c polarized protons stored in COSY. After optimizing the spin-flip parameters, we obtained a $99.92 \pm 0.04\%$ measured spin-flip efficiency [32]. This is consistent with the earlier obtained proton spin-flip efficiency of $99.93 \pm 0.02\%$ at 0.49 GeV/c at IUCF [22]. An rf-dipole's $\int Bdl$ is Lorentz invariant and its resonance strength becomes almost energy-independent at high energy. Thus, if no new problems emerge, even a small rf dipole with an $\int Bdl$ of about 0.6 T·mm should allow more than 99.9% proton spin-flip efficiency in Brookhaven's 250 GeV Relativistic Heavy Ion Collider (RHIC) and perhaps someday in CERN's 7 TeV Large Hadron Collider (LHC).

We next compiled [33] all then-existing data on the spin-manipulation of polarized stored beams of protons, deuterons and electrons using the horizontal rf magnetic field of either an rf dipole or solenoid. We then fit these polarization data to the Froissart-Stora equation to obtain the measured rf spin resonance strength ε_{FS}. We also calculated for each data set the corresponding strength ε_{Bdl} from the $\int Bdl$ of the rf magnet used for the spin-manipulation by using the widely-accepted formulae for ε_{Bdl} [43, 44, 45]. We found deviations in the $\varepsilon_{FS}/\varepsilon_{Bdl}$ ratio, which should be 1, by factors of up to 7 or more in each direction. All the $\varepsilon_{FS}/\varepsilon_{Bdl}$ ratios for rf dipoles with protons seemed to be above 1. All the rf-dipole $\varepsilon_{FS}/\varepsilon_{Bdl}$ ratios with deuterons were far below 1, but they also had small frequency ramp ranges Δf. The single rf

solenoid point with deuterons had $\varepsilon_{FS}/\varepsilon_{Bdl}$ very near 1; moreover the two rf solenoid points with protons had $\varepsilon_{FS}/\varepsilon_{Bdl}$ near or below 1.

To understand these deviations, we studied them experimentally at COSY using an rf dipole with both protons and deuterons, and using an rf solenoid with deuterons. We first used the rf dipole magnet to spin-manipulate the polarization of a 2.1 GeV/c vertically polarized proton beam, while varying the rf dipole's voltage, and the beam's size and vertical betatron tune [33]. We saw a linear dependence of the rf spin resonance strength ε_{FS} on the rf dipole's voltage. We found no dependence of ε_{FS} on the beam's vertical size; however, we found even larger deviations of $\varepsilon_{FS}/\varepsilon_{Bdl}$, of more than 100, when the rf spin resonance was moved near an intrinsic spin resonance by changing COSY's vertical betatron tune ν_y. This enhancement near an intrinsic resonance seems to explain why the $\varepsilon_{FS}/\varepsilon_{Bdl}$ ratio was always higher than 1 for protons. This effect had been seen earlier [47, 48] but only very near an intrinsic resonance; it was apparently not understood that the enhancement would be so large far from an intrinsic resonance.

We next manipulated the polarization of a 1.85 GeV/c vertically polarized deuteron beam using the same rf dipole [33, 34]. We varied the rf dipole's voltage and frequency ramp range, and the beam's size, momentum spread and vertical betatron tune. We observed a linear dependence of the rf spin resonance strength ε_{FS} on the dipole's voltage, and no dependence on its frequency ramp range. We also found no dependence of ε_{FS} on the beam's vertical size or momentum spread. When the rf resonance was near an intrinsic spin resonance, we found an enhancement of about 20 over the flat "base-line" ε_{FS} away from the intrinsic resonance. Thus, destructive interference with an intrinsic resonance could not explain the 7-fold reduction of ε_{FS} for deuterons.

We recently built an rf solenoid magnet to study its spin resonance strength at COSY. We used it to manipulate the polarization of a 1.85 GeV/c vertically polarized deuteron beam, while varying the rf solenoid's frequency ramp range Δf, and the deuteron beam's momentum spread $\Delta p/p$ and vertical betatron tune ν_y. We saw no ε_{FS} dependence on the solenoid's Δf, or on the beam's $\Delta p/p$ or ν_y. Moreover, the $\varepsilon_{FS}/\varepsilon_{Bdl}$ ratio was very close to 1, except for the single point centered exactly on the intrinsic resonance [78]. This confirmed the widely used formula for the spin resonance strength due to an rf solenoid with its $(1+G)$ factor; it also increased the concern about the experimental disagreement with the equally widely used $(1+G\gamma)$ factor in the rf dipole formula.

These studies inspired a theoretical discussion of the formula for the rf spin resonance strength due to an rf dipole. Kondratenko suggested [79] that in an "ideal" circular accelerator or storage ring with no radial or longitudinal magnetic fields, except for a short rf dipole, the factor $(1+G\gamma)$ should instead be close to $G\gamma$. However,

radial and longitudinal fields are always present in real accelerators or storage rings; thus, this factor is instead a complex function, which must be calculated for each ring's actual parameters. Therefore, in any real accelerator the factor is neither $G\gamma$ nor $(1 + G\gamma)$.

Studying these deviations also helped to inspire a new analytic formalism by Chao [75], which seems to be the first generalization of the Froissart-Stora equation [17] since its publication in 1960. Chao's analytic Matrix Formalism was recently confirmed experimentally [76, 77].

BIBLIOGRAPHY

BIBLIOGRAPHY

[1] B. v. Przewoski et al., Phys. Rev. C 58, 1897 (1998).

[2] P.K.A. De Witt Huberts, Nucl. Phys. A 553, 845C (1993).

[3] R. Alarcon et al., (BLAST Collaboration), in MIT Bates Report No. 2-39 (1999).

[4] H. Rohdjess et al., AIP Conf. Proc. No. 675 (AIP, New York, 2003), p. 523.

[5] A. Assmann et al., AIP Conf. Proc. No. 343 (AIP, New York, 1995), p. 219.

[6] Y. Makdisi, AIP Conf. Proc. No. 343 (AIP, New York, 1995), p. 75.

[7] A.D. Krisch et al., (SPIN Collaboration), University of Michigan Reports No. UM-HE 96-20 (1996) and No. UM-HE 99-05 (1999); A. Airapetian et al., (HERMES Collaboration), DESY-PRC Report No. 99-08 (1999).

[8] T. Khoe *et al.*, Part. Accel. **6**, 213 (1975).

[9] F.Z. Khiari *et al.*, Phys. Rev. D **39**, 45 (1989).

[10] J.L. Laclare *et al.*, Jour. de Phys. **46**, C2-499 (1985).

[11] H. Sato *et al.*, Nucl. Instrum. Methods A **272**, 617 (1988).

[12] Ya.S. Derbenev and A.M. Kondratenko, Part Accel. **8**, 115 (1978).

[13] A.D. Krisch *et al.*, Phys. Rev. Lett. **63**, 1137 (1989).

[14] J.E. Goodwin *et al.*, Phys. Rev. Lett. **64**, 2779 (1990).

[15] I. Alekseev *et al.*, Nucl. Instrum. Methods Phys. Res., Sect. A **499**, 392 (2003).

[16] M. Bai *et al.*, Phys. Rev. Lett. **96**, 174801 (2006).

[17] M. Froissart and R. Stora, Nucl. Instrum. Methods **7**, 297 (1960).

[18] V.A. Anferov *et al.*, Phys. Rev. ST Accel. Beams **3**, 041001 (2000).

[19] B.B. Blinov *et al.*, Phys. Rev. ST Accel. Beams **3**, 104001 (2000).

[20] A.M.T. Lin *et al.*, in *SPIN 2000: 14th International Spin Physics Symposium, Osaka, 2000*, edited by K. Hatanaka, AIP Conf. Proc. No. 570 (AIP, Melville, NY, 2001), p. 736.

[21] Michigan-IUCF SISN Run, 2001 (unpublished).

[22] B.B. Blinov *et al.*, Phys. Rev. Lett. **88**, 014801 (2002); V.S. Morozov *et al.*, in *SPIN 2002: 15th International Spin Physics Symposium, Upton, NY, 2002*, edited by Y.I. Makdisi *et al.*, AIP Conf. Proc. No. 675 (AIP, Melville, NY, 2003), p. 776.

[23] V.S. Morozov *et al.*, Phys. Rev. ST Accel. Beams **7**, 024002 (2004).

[24] A.D. Krisch *et al.*, in *SPIN 2004: 16th International Spin Physics Symposium, Trieste, Italy, 2004*, edited by K. Aulenbacher it et al. (World Scientific, Singapore, 2005), p. 691.

[25] D.D. Caussyn *et al.*, Phys. Rev. Lett. **73**, 2857 (1994).

[26] D.A. Crandell *et al.*, Phys. Rev. Lett. **77**, 1763 (1996).

[27] B.B. Blinov *et al.*, Phys. Rev. Lett. **81**, 2906 (1998); V.A. Anferov *et al.*, in *Proceedings of the 13th International Symposium on High Energy Spin Physics (IHEP), Protvino, Russia, 1998*, edited by N.E. Tyurin *et al.* (World Scientific, Singapore, 1999), p. 503.

[28] V.S. Morozov *et al.*, Phys. Rev. Lett. **91**, 214801 (2003).

[29] K. Yonehara *et al.*, in *Proceedings of the 8th Conference on the Intersections of Particle and Nuclear Physics, New York, NY, 2003*, edited by Z. Parsa, AIP Conf. Proc. No. 698 (AIP, Melville, NY, 2003), p. 763.

[30] V.S. Morozov *et al.*, Phys. Rev. ST Accel. Beams **8**, 061001 (2005).

[31] V.S. Morozov *et al.*, Phys. Rev. ST Accel. Beams **4**, 104002 (2001).

[32] M.A. Leonova *et al.*, Phys. Rev. Lett. **93**, 224801 (2004).

[33] M.A. Leonova *et al.*, Phys. Rev. ST Accel. Beams **9**, 051001 (2006).

[34] A.D. Krisch *et al.*, Phys. Rev. ST Accel. Beams **10**, 071001 (2007).

[35] A.W. Chao, *Special Topics in Accelerator Physics*, US Particle Accelerator School, SUNY Stony Brook (2000).

[36] S.Y. Lee, *Spin Dynamics and Snakes in Synchrotrons*, (World Scientific, Singapore, 1997).

[37] L.H. Thomas, Philos. Mag. **3**, 1 (1927).

[38] V. Bargmann, L. Michel and V.L. Telegdi, Phys. Rev. Lett. **2**, 435 (1959).

[39] E.D. Courant, Bull. Am. Phys. Soc. **7**, 33 (1962) and Rpt. BNL-EDC-45 (1962).

[40] B.W. Montague, Phys. Rep. **113**, 1 (1984).

[41] E.D. Courant and R.D. Ruth, *Accel. Polarized Protons in Circular Accelerators*, BNL Rpt. 51270 (1980).

[42] H. Stockhorst, B. Lorentz, COSY Internal Rpt. (2003).

[43] T. Roser, *Handbook of Accelerator Physics and Engineering*, edited by A.W. Chao and M. Tigner (World Scientific, Singapore, 2006), p. 170, Eqs. (6) and (7).

[44] S.Y. Lee, Phys. Rev. ST Accel. Beams **9**, 074001 (2006).

[45] M. Bai *et al.*, Phys. Rev. ST Accel. Beams **8**, 099001 (Sept 2005).

[46] V.S. Morozov *et al.*, Phys. Rev. ST Accel. Beams **8**, 099002 (2005).

[47] M. Bai *et al.*, Phys. Rev. E **56**, 6002 (1997).

[48] Ya.S. Derbenev and V.A. Anferov, Phys. Rev. ST Accel. Beams **3**, 094001 (2000).

[49] A. Schnase, et. al., "RF-Dipole System at COSY for spin-flipping experiments", IKP Annual Report 2002

[50] P.D. Eversheim *et al.*, in *Proceedings of the 8th International Symposium on Polarization Phenomena in Nuclear Physics, Bloomington, IN, 1994*, edited by Edward J. Stephenson and Steven E. Vigdor, AIP Conf. Proc. No. 339 (AIP, Woodbury, NY, 1995), p. 668.

[51] R. Weidmann *et al.*, Rev. Sci. Instrum. **67**, 1357 (1996).

[52] O. Felden *et al.*, in *Proceedings of the 9th International Workshop on Polarized Sources and Targets, Nashville, IN, 2001*, edited by V.P. Derenchuk and B. von Przewoski (World Scientific, Singapore, 2002), p. 200.

[53] W. Bräutigam *et al.*, in *Proceedings of the 15th International Conference on Cyclotrons and Their Applications, Caen, France, 1998*, edited by E. Baron and M. Lieuvin (IOP Publishing, Bristol, 1999), p. 654.

[54] W. Bräutigam *et al.*, in *Proceedings of the 16th International Conference on Cyclotrons and Their Applications, East Lansing, MI, USA, 2001*, edited by F. Marti, AIP Conf. Proc. No. 600 (AIP, Melville, NY, 2001), p. 123.

[55] W. Bräutigam *et al.*, in *Proceedings of the XXXIII European Cyclotron Progress Meeting, Warsaw, Poland, 2002* (Nukleonika vol. **48**, suppl. 2, 2003), p. s123.

[56] D. Chiladze *et al.*, Phys. Rev. ST Accel. Beams **9**, 050101 (2006).

[57] R. Maier, Nucl. Instrum. Methods Phys. Res., Sect. A **390**, 1 (1997).

[58] A. Lehrach *et al.*, in *Proceedings of the 1999 Particle Accelerator Conference, New York, NY, 1999*, edited by A.U. Luccio and W.W. MacKay (IEEE, Piscataway, NJ, 1999), p. 2292.

[59] H. Stockhorst *et al.*, in *Proceedings of the 8th European Particle Accelerator Conference, Paris, 2002* (EPS-IGA/CERN, Geneva, 2002), p. 629.

[60] A. Lehrach *et al.*, in *SPIN 2002: 15th International Spin Physics Symposium, Upton, NY, 2002*, edited by Y.I. Makdisi *et al.*, AIP Conf. Proc. No. 675 (AIP, Melville, NY, 2003), p. 153.

[61] H. Stein *et al.*, Atomic Energy, **94**, 1 (2003), p. 24.

[62] M. Altmeier *et al.* (EDDA Collaboration), Phys. Rev. Lett. **85**, 1819 (2000).

[63] D. Albers *et al.*, Eur. Phys. J. A **22**, 125 (2004).

[64] M. Altmeier *et al.*, Eur. Phys. J. A **23**, 351 (2005).

[65] F. Bauer *et al.*, Phys. Rev. C **71**, 054002-1 (2005).

[66] M.A. Leonova, SPIN@COSY internal report, 2003 (unpublished).

[67] A. Schnase *et al.*, *"Ferrite loaded RF-Dipole for Spin-manipulation of Protons and Deuterons"*, in Forschungszentrum Jülich Institut für Kernphysik Annual Report 2003.

[68] M.A. Leonova, SPIN@COSY internal report, 2007 (unpublished).

[69] H. Stockhorst *et al.*, SPIN@COSY internal report, 2007 (unpublished).

[70] V. Schwarz, Ph.D. dissertation, Universität Bonn (1999).

[71] K. Sekiguchi *et al.*, Phys. Rev. C **65**, 034003 (2002).

[72] M. Haji-Saied *et al.*, Phys. Rev. C **36**, 2010 (1987).

[73] H. Rohdjess, SPIN@COSY internal report, 2004 (unpublished).

[74] V.S. Morozov, Ph.D. dissertation, University of Michigan (2007).

[75] A.W. Chao, Phys. Rev. ST Accel. Beams **8**, 104001 (2005).

[76] V.S. Morozov *et al.*, Phys. Rev. ST Accel. Beams **10**, 041001 (2007).

[77] V.S. Morozov *et al.*, Phys. Rev. Lett. **100**, 054801 (2008).

[78] M.A. Leonova *et al.*, to be submitted for publication.

[79] A.M. Kondratenko, SPIN@COSY Internal Rpt., August 2006; *ibid.* February 2007; *Proc.* 9^{th} *Intl. Symposium on High Energy Spin Physics, Bonn, 1990* (Springer-Verlag, Berlin, 1991), p. 140; *Proc. VI Workshop on High Energy Spin Physics, Protvino, 1995* (Protvino, 1996), p. 207.